**Daniel Schmid, BSc**

# A statistical and event study of magnetotail dipolarization fronts

## MASTER THESIS

For obtaining the academic degree
Diplom-Ingenieur

Master Programme of
Technical Physics


**Graz University of Technology**

Supervisor:
Ao.Univ.-Prof. Dipl.-Ing. Dr.phil. Martin Heyn
Institute of Theoretical and Computational Physics

Graz, March 2012

Deutsche Fassung:
Beschluss der Curricula-Kommission für Bachelor-, Master- und Diplomstudien vom 10.11.2008
Genehmigung des Senates am 1.12.2008

## EIDESSTATTLICHE ERKLÄRUNG

Ich erkläre an Eides statt, dass ich die vorliegende Arbeit selbstständig verfasst, andere als die angegebenen Quellen/Hilfsmittel nicht benutzt, und die den benutzten Quellen wörtlich und inhaltlich entnommenen Stellen als solche kenntlich gemacht habe.

Graz, am …… ……..
(Unterschrift)

Englische Fassung:

## STATUTORY DECLARATION

I declare that I have authored this thesis independently, that I have not used other than the declared sources / resources, and that I have explicitly marked all material which has been quoted either literally or by content from the used sources.

…… ……..
date (signature)

## Abstract

The Earth's magnetotail is created through the interaction of the solar wind magnetoplasma and the Earth's internal magnetic field. The magnetic field lines, after reconnection at the dayside of the Earth, are dragged along with the solar wind and create the stretched magnetic fields that are observed as the Earth's magnetotail. This magnetotail is prone to many (explosive) instabilities, due to the stored magnetic energy, and shows various behaviours, most often instigated by magnetic reconnection in the tail. Magnetic reconnection in the tail re-connects the magnetic field lines from a stretched open configuration to a stretched closed configuration, where the stored magnetic energy is released through the magnetic tension of the field and the field lines move back to Earth, accelerating plasma Earthward at the same time. In this way the magnetic energy is converted to kinetic energy of the plasma. This creates a so-called Bursty Bulk Flow (BBF), short-duration high-velocity plasma flows towards the Earth. These BBFs are often accompanied by magnetic field dipolarizations, i.e. the Z-component of the magnetic field increases while the X-component decreases, and the field looks more like that of a magnetic dipole than like the stretched magnetotail. However, it is not just a simple turning of the field form X into Z, for example, it has been observed in experimental data that the increase of the Z-component is preceded by a decrease and often there is an overshoot of the Z-component. It is this turning of the magnetic field that is studied in detail using the data from the CLUSTER mission.



## Abstract

Durch die Wechselwirkung des Magnetfeldes der Sonne mit dem Magnetfeld der Erde entstehen dynamische Effekt in der Magnetosphere. Die Magnetfeldlinien auf der Tagseite der Erde können sich mit den Magentfeldlinien der Sonne 'neuverbinden' und anschliessend mit dem Sonnenwind auf die Nachtseite transportiert werden. So entsteht der weit auseinandergezogene und dadurch sehr instabile Magnetschweif der Erde. Da ständig neue Magentfeldlinen von der Tagseite in den Magenetschweif gebracht werden, erhöht sich dort die magnetische Energie. Aufgrund der erhöhten Energie kann es dann zu einer erneuten 'Rekonnexion' der Magenetfeldlinien kommen. Die jetzt geschlossenen magnetischen Feldlinien versuchen die durch die Dehnung erzeugte zusätzliche Energie zu verringern und bewegen sich deshalb wieder Richtung Erde. Dabei wird Plasma aus dem Magnetschweif mitbeschleunigt und ein sogenannter 'Bursty Bulk Flow' (BBF) entsteht. Diese kurzzeitigen, sehr schnellen Plasmabewegungen Richtung Erde sind häufig mit einer so genannten 'Magnetschweif Dipolarisierung' verbunden. Das heisst, dass sich die normalerweise horizontal verlaufenden Magnetfeldlinien im Magnetschweif plötzlich in vertikale Richtung drehen und die Feldlinien eine dipolähnliche Form einnehmen. Mit Hilfe der Daten der CLUSTER Mission wurde dieses Phänomen genauer untersucht.

## Zusammenfassung

Im Zuge dieser Diplomarbeit wurden die 'Magnetschweif Dipolarisierungen', die von den CLUSTER Satelliten in einer Entfernung von $-20\ R_E \leq X_{GSM} \leq -10\ R_E$, $|Y_{GSM}| \leq 12\ R_E$ und $|Z_{GSM}| \leq 5\ R_E$ zur Erde beobachtet wurden, charakterisiert und untersucht. Anhand spezieller Kriterien für die Plasma- und Magnetfelddaten wurden die 'Dipolarisierungen' automatisch gesucht. Insgesamt wurden 107 'Dipolarisierungen' gefunden. Um die Abhängigkeit der 'Dipolarisierungsdauer' von der Plasmageschwindigkeit zu untersuchen, wurden diese Events statistisch ausgewertet. Anschliessend wurde anhand der Messdaten aller vier CLUSTER Satelliten die durchschnittliche räumliche Ausdehnung der 'Dipolarisierungen' analysiert. Für 24 der 107 gefunden 'Dipolarisierungen' konnte die Breite der magnetischen Struktur, in dem das Plasma 'eingefroren' ist, berechnet werden. Zum Schluss wurde anhand von zwei Beispielen, mit unterschiedlichem zeitlichen Verlauf, die durch die 'Dipolarisierung' entstehenden Ströme berechnet und mit den aus den Messdaten ermittelten diamagnetischen Strömen verglichen.

1. Es konnte gezeigt werden, dass mit zunehmender Plasmageschwindigkeit die Dauer der 'Dipolarisierung' abnimmt. Je höher die Plasmageschwindigkeit, desto schneller dreht das normalerweise horizontal verlaufende Magnetfeld im Magentschweif in vertikaler Richtung.
2. Die räumliche Ausdehnung einer 'Dipolarisierung' scheint von der Plasmageschwindigkeit unabhängig zu sein und beträgt im Durchschnitt $\sim 450 \pm 350$ km. Das entspricht in etwa der berechneten durchschnittlichen Inertiallänge der Ionen ($\sim 340 \pm 60$ km) und dem durchschnittlichen Gyroradius der Ionen ($\sim 590 \pm 150$ km).
3. Offentsichtlich fliessen die berechneten Ströme auf der 'Dipolarisierungs-Front' in die selbe Richtung wie die von CLUSTER beobachteten diamagnetischen Ströme und zwar normal zum Magnetfeld. Dies führt zum Schluss, dass 'Dipolarisierungs-Fronten' tangentiale Unstetigkeiten sind.

**Acknowledgments**

First of all I would like to express my deepest thanks to *Dr. Martin Volwerk* and *Dr. Rumi Nakamura* for there excellent supervision and support during my stay at the *Space Research Institute* in the *Austrian Academy of Sciences* in Graz. I owe my deepest gratitude especially to *Dr. Volwerk* for his great educational efforts and the vast amount of time he spent with me discussing all the stuff related to this thesis. It is also an honor for me that I had the opportunity to learn from the leading scientists in the field of magnetosphere dynamics, in particular *Prof. Wolfgang Baumjohann*, the director of the Institute, and his outstanding scientific knowledge.

This thesis would not have been possible unless my supervisor *Prof. Martin Heyn*. I had the opportunity to learn from his excellent analytical knowledge when conducting final discussions about the correction of my thesis.

I am also very greatful to my parents, *Othmar* and *Theresia Schmid* who encouraged me during all the years of study in Graz and supported me as much as possible.

I am also indebted to many of my colleagues who became close friends here in Graz, while spending nights of discussions and debates about physics. Furthermore I would like to thank all of my friends at home in Seefeld who supported me all the time.

Finally I acknowledge the *Cluster Science Data System* (CSDS) and the *Cluster Active Archive* (CAA) for data processings.

# Contents

# List of Figures

# List of Tables

# Chapter 1

# Introduction

## 1.1 Purpose

The Earth's magnetotail is created through the interaction of the solar wind magnetoplasma and the Earth's internal magnetic field. The magnetic field lines, after reconnection at the dayside of the Earth, are dragged along with the solar wind and create the stretched magnetic fields that are observed as the Earth's magnetotail. This magnetotail is prone to many (explosive) instabilities, due to the stored magnetic energy, and shows various behaviours: flapping [Sergeev et al. [28]]; evacuation [Volwerk et al. [35]]; kinking [Volwerk et al. [34]]; etc., most often instigated by magnetic reconnection in the tail. Magnetic reconnection in the tail re-connects the magnetic field lines from a stretched open configuration to a stretched closed configuration, where the stored magnetic energy is released through the magnetic tension of the field and the field lines move back to Earth, accelerating plasma Earthward at the same time. In this way the magnetic energy is converted to kinetic energy of the plasma. This creates a so-called Bursty Bulk Flow (BBF) [Angelopoulos et al. [3]], short-duration high-velocity plasma flows towards the Earth. These BBFs are often accompanied by magnetic field dipolarizations, i.e. the $Z$-component of the magnetic field increases while the $X$-component decreases, and the field looks more like that of a magnetic dipole than like the stretched magnetotail. However, it is not just a simple turning of the field form $X$ into $Z$, for example, it has been observed in experimental data that the increase of the $Z$-component is preceded by a decrease and often there is an overshoot of the $Z$-component. It is this turning of the magnetic field that is proposed to be studied in detail using the data from the Cluster mission.
The Cluster mission [Escoubet et al. [11]] was launched in 2000 and consists of four equal satellites in a polar orbit around the Earth. This is the first dedicated multi-point measurement mission. In regions of interest in the Earth's magnetosphere, e.g. during crossing of the magnetotail, the spacecraft were in a tetrahedral configuration. On all spacecraft the magnetic field is measured with flux gate magnetometers [Balogh et al. [5]] and on three of the four spacecraft there is an operational plasma instrument

[Rème et al. [24]]. All data for this mission are now available through the Cluster Active Archive website.
As mentioned above, magnetotail dipolarizations, i.e. the northward turning of the magnetic field in the magnetotail is most often observed during BBFs created by magnetic reconnection down the tail. Two statistical analyses have been performed on Geotail [Ohtani et al. [22]] and data from Wind [Sigsbee et al. [30]]. The important characteristics obtained from these studies are:

- The magnetic field becomes dipolar in the course of the fast earthward flow;
- Sharp dipolarization tends to be preceded by a transient decrease in $B_Z$, which starts along with the fast flow and is accompanied by an increase in the plasma density;
- The plasma and total pressures decrease in the course of the fast flow, suggesting the reduction of the lobe field strength.

Interestingly, the decrease in Bz can be so strong that this field component changes sign and becomes negative, something that in principle is not expected on closed, Earthward moving field lines.
The four spacecraft tetrahedron configuration of Cluster makes it possible to measure gradients in the magnetic field and other parameters. The gradients in the magnetic field can be used to calculate e.g. the currents that are flowing in the magnetotail at the location of the tetrahedron, something previous experiments were unable to do. Using the four Cluster spacecraft to do timing analysis [Harvey [12]], it is possible to obtain the velocity of the magnetic structure, under the assumption that the structure is a propagating plane.
In this master thesis we will use these techniques to obtain the thickness of the dipolarization fronts and the associated currents.

## 1.2 Description of Content

At the beginning a short survey of the physical basics with regard to this master thesis will be given. Therefor chapter 2 is split into two sections, section 2.1 provides a brief introduction into space physics, based on a mixture of simple theory and a description of the wealth of space plasma phenomena and section 2.2 presents a general overview of the Cluster mission, the instruments of the Cluster spacecraft and the dataset of Cluster's observations.
However, chapter 2 should show the basic principles for undergraduated students of physics, who have an average knowledge of fluid dynamics and electromagnetism. Research and advanced readers may find chapter 3 more interesting. There a more rigourous theoretical understanding of space plasma physics and particularly in magnetotail physics should be present. The first section in chapter 3 (section 3.1) gives a

short introduction of magnetotail dipolaritzations. In section 3.2 the selection criteria for finding such dipolarization events will be introduced. In section 3.3 a 'typical' dipolarization event will be shown and discussed. Also a statistical analysis (superposed epoch study) of all found events will be conducted. In section 3.4 multi-spacecraft studies will be performed, to obtain more accurate information about the characteristics of dipolarization events such as the spatial or temporal scale of the dipolarization front. In the last section of chapter 3 (section 3.5) the dipolarization-associated currents in the magnetotail will be determined to verify the estimated results of section 3.3.
In chapter 4 all results of chapter 3 will be discussed and the key results will be summarised. This master thesis supposed to be written in a self-containing way so that the reader can follow without need to consult original sources. Hereby the basic steps of derivation are presented in the text and some of the more involved mathematical derivations are given in the Appendix.

# Chapter 2

# Basic Information

Space physics is a subject of geophysics and is unique form other fields of astrophysics which study similar phenomena, in that way that space physics utilises in-situ measurements from high altitudes, i.e., rockets and spacecraft. In the fifties the key interests of geophysics was the interior of our planet, i.e., seismology, rock physics, etc. With the era of space-flight, the interests of geophysicists broadened and extended into the external neighbourhood of our planet [6].
It was found that the extraterrestrial matter is in an ionised state, similar to gas in which a certain portion of particles are ionised. Matter of this kind is electrically conductive so that it is very sensitive to electric and magnetic fields. Within this context, the term of *plasma* became a new and important category of geophysics. Plasma are not abundant in the interplanetary space, but also in our solar system. Even in the near neighbourhood of the Earth, all matter above $\sim$ 100 km altitude, has to be treated using plasmaphysical methods. Nowadays, methods of plasma physics are not only used in extraterrestrial geophysics, but are essential to understand the physical background of the behaviour of plasma for industrial applications. In section 2.1 a few basic aspects of the space plasma physics which are relevant for this master thesis are presented.
For the investigation of magnetotail dipolarization the dataset of the Cluster spacecraft are utilized. Because the Cluster Mission consists of four identical spacecraft, 3-D, time-resolved measurements are possible and the small-scale structures in space and time can be studied. In the second part of this chapter (section 2.2) a general overview of the Cluster Mission and the payload of instruments which are relevant for this master thesis are given.

## 2.1 Space Plasma Physics Background

### 2.1.1 Definition of Plasma

A *plasma* is a gas of charged particles in a *quasi-neutral* state. That means the plasma consists of equal numbers of free positive and negative charge carriers in the same volume element.
Only for particles with an random kinetic (thermal) energy much higher than the potential energy, the motion is practically free from the influence by other charged particles as long as no direct collisions take place. Since the particles in a plasma have to overcome the coupling with their neighbours, they must have thermal energies above some electronvolts [6].
Typical parameters characterizing a plasma are:

**Debye Shielding:**

Let the plasma be macroscopic electrical neutral, the electric Coulumb potential field of every charge, $q$

$$\phi_C = \frac{q}{4\pi\varepsilon_0 r} \tag{2.1}$$

with $\varepsilon_0$ the free space permittivity, is shielded by other charges in the plasma and assumes the *deby potential* form

$$\phi_D = \frac{q}{4\pi\varepsilon_0 r} exp(-\frac{r}{\lambda_D}) \tag{2.2}$$

in wich the exponetial function cuts off the potential at distances $r > \lambda_D$. $\lambda_D$ is called *Debye length* and is the distance, over which charge carriers screen out electric fields in plasmas. Comparison between the thermal energy $k_B T_e$ and the potential energy $|e\phi|$ in an area where charge seperation ($n_i \approx n_e \equiv n$) is obtained, gives

$$\frac{ne^2}{\varepsilon_0}\lambda_D^2 = k_B T_e$$

$$\boxed{\lambda_D = \sqrt{\frac{\varepsilon_0 k_B T_e}{ne^2}}} \tag{2.3}$$

In order for a plasma to be quasineutral, the physical dimension of the system, L, must be large comparred to $\lambda_D$. Otherwise there is not enough space for the collective shielding effect to occur, and a simple ionized gas remains [6].

**Plasma Parameter:**

Since the Debye shielding is a collective effect, a lot of particles have to participate at the same time. In other words, a lot of particles have to be located inside the

Debyesphere of a radius $\lambda_D$. The number of particles $N$ inside this sphere is given by

$$N = \frac{4\pi}{3} n_e \lambda_D^3$$

where

$$\Lambda = n_e \lambda_D^3 \tag{2.4}$$

is often called the *plasma parameter*. However, this is only possible if the electrostatic Coulomb-interaction between the particles is much smaller than the thermal energy, which determinate the size of the Debyesphere.
Somtimes instead of $\Lambda$ it's reciprocal $g$ is defined as the plasma parameter with the **Weak Coupling Condition**,

$$\boxed{g \equiv \frac{1}{n_e \lambda_D^3} \ll 1} \tag{2.5}$$

Typical conditions of the characteristic lengths for geophysical plasmas:

| | quasi-neutrality | | weak-coupling | |
|---|---|---|---|---|
| L | $\gg$ | $\lambda_D$ | $\gg$ | l |
| physical dimension of the system | | Debye-length | | interparticles distiance |

Table 2.1: Typical conditions for several geophysical plasmas [1].

where $l \sim n_e^{1/3}$.

**Plasma Frequency:**

Another important plasma criteria is the *plasma frequency* $\omega_P$. It is the typical oscillation frequency of a fully ionized plasma when its equilibrium is disturbed by an external force [6]. Due to the external force, the electrons begin to oscillate around the heavier ions, in attempt to restore the quasi-neutrality.

$$\boxed{\omega_P = \sqrt{\frac{n_e e^2}{m_e \varepsilon_0}}} \tag{2.6}$$

However, for not fully ionized plasma, collisions with neutral particles damp the collective oscillation of the electrons and hence the collective behaviour of the plasma is defected. So a not fully ionized medium has to fulfil the criteria

$$\omega_P \cdot \tau_n \gg 1 \tag{2.7}$$

where $\tau_n$ is the average collisions time with neutral particles, to behave as a plasma.

[1] [Source: [13]]

### 2.1.2 The Earth's Magnetosphere

The Earth's magnetosphere is basically composed of two essential ingredients. The first is the intrinsic magnetic field of the Earth, generated by currents flowing in Earth's core. This currents arise form the circulation of liquid metal in the core, driven by internal heat sources. Outside the Earth this magnetic field resemble the dipole field of a bar magnet, aligned approximately with the Earth's spin axis. The cavity generated by the terrestrial field has been named *magnetosphere*.
The second ingredient is the solar wind, a fully ionized hydrogen/helium plasma that streams continuously outward from the sun into the solar system at speeds of $\sim 300 - 800$ km/s [31]. In simple terms, the flow exists because the sun's corona is hot ($\sim 10^6$ K) and the pressure in the local interstellar medium is far less than that in the corona. This plasma wind is pervaded by a large-scale interplanetary magnetic field (IMF), which is produced by stretched-out magnetic field lines originating on the sun. Because of the high conductivity of the plasma, the solar magnetic field is frozen in the plasma and drawn outward by the expandig solar wind. The IMF plays an important role in the Earth's magnetic field interaction with the solar wind (see e.g. subsection 2.1.4).
There is also a third ingredient that is important for the formation of the Earth's magnetosphere: the Earth's ionosphere. Above altitudes of $\sim$ 100 km the upper atmosphere is partly ionized by solar radiation (far-ultraviolet and X-rays). The Ionosphere forms a second source of plasma for the magnetosphere, mostly of protons and singly charged helium and oxygen.
When the solar wind hits on the Earth's terrestrial magnetic field, it cannot easily penetrate it but is slowed down and largely deflected around it hence a bow shock wave is generated. This is because of the fact that the IMF cannot simply penetrate the Earth's magnetic field and the particles of the sun wind cannot leave the IMF due to the frozen-in characteristic of the conductive plasma. The plasma is slowed down and due to the substantial fraction of the particles, kinetic energy converts into thermal heat. The region of this subsonic plasma behind the bow shock is call *magnetosheath*. The boundary which separates the magnetosheath and the magnetosphere is called *magnetopause*. In Figure 2.1 the topography of the solar-terrestrial environment with the different regions are shown [6].

Now then, the kinetic pressure of the sun wind deforms the outer part of the terrestrial magnetic field. The frontside of the field gets compressed, while the nightside is stretched out into the so called *magnetotail* (see Figure 2.1). The Earth's magnetic tail extends at least 200 $R_E$ (Earth radii) [6].
The plasma inside the magnetosphere consists mostly of electrons and protons from the solar wind and the ionosphere. But there is a small number of $He^+$ and $O^+$ ions which derive from the ionosphere and a few $He^{++}$ ions originating from the solar wind. The plasma in the magnetosphere is not equally distributed, but it is sub-diveded into different regions with different plasma properties like pressure and temperature (see Ta-

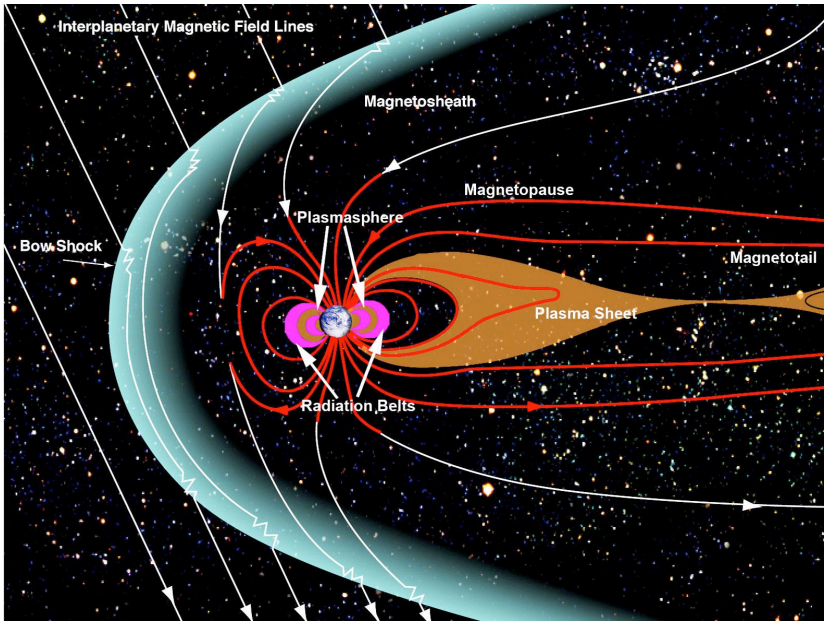


Figure 2.1: Topography of the solar-terrestrial environment and the plasma structure of the Earth's magnetosphere [3].

ble 2.2). In Figure 2.1 some of this regions are shown. The *radiation belt* or *Van Allen radiation belt* consists of energetic particles which oscillate back and forward along the dipolar field lines. In the strict sence there are two radiaton belts. An outer radiation belt which extends form an altitude around 2 and 6 $R_E$ and an inner radiation belt which reaches an altitude of maximum 1.5 $R_E$.
Inside the outer radiation belts is the *plasmasphere*. It contains cool but dense plasma of ionospheric origin, which corotates with the Earth.
Most of the magnetotail plasma is concentrated in the so called *plasmasheet*. The plasmasheet lies in the midplane of the tail and is about 10 $R_E$ thick and reaches down to the high-latitude auroral ionosphere along the field lines. The plasma sheet splits the outer part of the magnetotail into the nothern and southern *magnetotail lobe*.

| **Region** | **Range [$R_E$]** | $T_e^-$ **[K]** | $n_e^-$ **[$cm^{-3}$]** | **B [nT]** |
|---|---|---|---|---|
| Solar Wind and IWF | | $10^5$ | 5 | 5 |
| Magnetotail Lobe | | $5 * 10^5$ | $10^{-2}$ | 30 |
| Plasma Sheet | 10 | $5 * 10^6$ | 0.5 | 10 |
| Radiation Belt | 2 - 6 | $5 * 10^7$ | 1 | 100 - 1000 |
| Plasmasphere | 4 | $5 * 10^3$ | $5 * 10^2$ | > 1000 |

Table 2.2: Typical parameters for several geophysical plasmas [4].

[3] [Source: http://www.nasa.gov]
[4] [Source: [6]]

### 2.1.3 Currents in the Magnetosphere

The deformation of the magnetosphere due to the distortion of the terrestrial dipole filed by the solar wind is accompanied by electrical currents. In Figure 2.8 the currents that flow in the different magnetosphere regions are schematically shown.

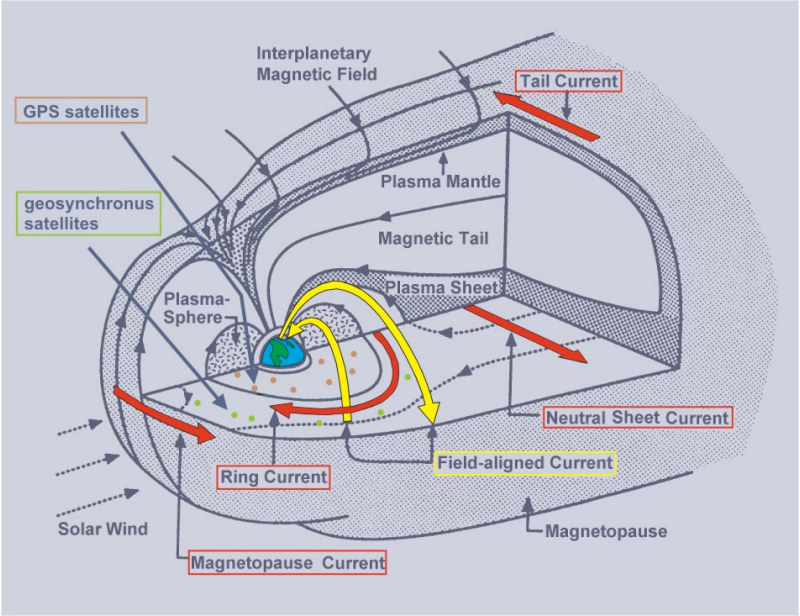


Figure 2.2: Synopsis of magnetospheric currents. Additional the radial distances of geosynchronous and gps satellites are plotted [6].

The compression of the magnetosphere on the frontside is associated with a current flow across the surface of the magnetopause the *magnetopause current*.The stretched field of the nightside magnetosphere is accompanied with current flow on the surface of the magnetotail the *tail current*. In the central plasma sheet the so called *neutral sheet current* is flowing [6].
Another large-scale current system is the *ring current*. This current flows clockwise around the Earth at radial distances of a few Earth radii and is generated by the radiation belt particles which oscillate between the northern and southern hemisphere (see subsection 2.1.2). In addition to their bounce motion, these particles drift slowly around the Earth. The ring current influences the configuration to the inner magnetosphere. The particles of this region create a magnetic field that is contrary to the Earth's magnetic field hence the magnetic field in this area decreases.
Beside these perpendicular currents, currents also flow along magnetic field lines the *field aligned currents*. These currents are mainly carried by electrons and are essential for the exchange of energy and momentum between the magnetosphere and the ionosphere [6].

[6][Source: http://www.ngdc.noaa.gov]

### 2.1.4 Convection and Substorms

Plasma particles with near-zero energy (cold plasma) **do not** feel magnetic forces like energetic particles which move across the magnetic field lines under the influence of magnetic gradient and curvature forces. The cold plasma particles, in the absence of external electric fields, do not drift at all [7] but stay close to the field line they gyrate about. Even the more energetic particles will stay at their field lines when the magnetic field gradient or curvature is not to strong. This has an important consequence. Whenever a field line moves due to external forces, plasma tied to this field line also moves. The same is valid for a moving plasma. Because the plasma can not leave the field line, the plasma will transport the magnetic field line along with it. Hence the motion of the plasma and the flux tube (bundle of magnetic field lines) are closely related [6].

## Diffusion and Frozen Flux:

In order to study the transport of field lines and plasma more quantitatively, we may start with *Faraday's law*

$$\nabla \times \mathbf{E} = -\frac{\partial \mathbf{B}}{\partial t} \tag{2.8}$$

and eliminate the electric field by the simple form of the *generalized Ohm's law* [8]

$$\mathbf{j} = \sigma_0(\mathbf{E} + \mathbf{v} \times \mathbf{B}) \tag{2.9}$$

where we have used the *plasma conductivity*

$$\sigma_0 = \frac{n_e e^2}{m_e \nu_c} \tag{2.10}$$

$n_e$ is the electron density, $\nu_c$ the collisions frequency, $e$ the electron charge and $m_e$ is the electron mass.
The $\mathbf{v} \times \mathbf{B}$ term on the right hand-side of Equation 2.9 results from the Lorentz transformation, because the plasma may move with velocity $\mathbf{v}$ across a magnetic field $\mathbf{B}$.
Faraday's law turns then into

$$\nabla \times (\mathbf{v} \times \mathbf{B} - \mathbf{j}/\sigma_0) = -\frac{\partial \mathbf{B}}{\partial t} \tag{2.11}$$

[7] Unless the adiabatic invariants change due to collective effects like the *anomalous collisions*. Geophysical plasmas are fully ionized and hence collisionsless, in the sence that the Coulomb collision frequency is much lower than the plasma frequency. However, the plasma may become collisional again due to the collective interaction, in which th self generated fields of the particles take over a significant role in the scattering process. [6]

[8] The simple form of the generalized Ohm's law is valid in all fully ionized geophysical plasmas were the typical collision frequencies are extremely low and the plasma conductivity can be taken as near-infinite.

Using *Ampere's law*

$$\nabla \times \mathbf{B} = \mu_0 \mathbf{j} + \varepsilon_0 \mu_0 \frac{\partial \mathbf{E}}{\partial t} \tag{2.12}$$

without the $\partial \mathbf{E}/\partial t$ term and noting that $\nabla \cdot \mathbf{B} = 0$, we get a general induction equation for the magnetic field (for the differential relations see section A.3)

$$\boxed{\frac{\partial \mathbf{B}}{\partial t} = \nabla \times (\mathbf{v} \times \mathbf{B}) + \frac{1}{\mu_0 \sigma_0} \nabla^2 \mathbf{B}} \tag{2.13}$$

Apparently the magnetic field at a point in a plasma can be changed by a motion of the plasma described in the first term on the right-hand side in Equation 2.13. It can also be changed by diffusion due to the second term on the right-hand side.

**Magnetic Diffusion:** Asuming the plasma to be at rest, Equation 2.13 becomes a diffusion equation for the magnetic field

$$\frac{\partial \mathbf{B}}{\partial t} = D_m \nabla^2 \mathbf{B} \tag{2.14}$$

with the *magnetic diffusion coefficient* given by $D_m = \frac{1}{\mu_0 \sigma_0}$.
The magnetic field tends to diffuse across the plasma to smooth out any local inhomogeneities, if the resistence in the plasma is finite. In the absence of collision $\sigma_0 \to \infty$ and the diffusion time can become extremely long and the magnetic field is not able to diffuse efficiently across the plasma [6].

**Hydromagnetic Theorem:** In collisionless plasma the magnetic diffusion is negligible (see above) and one speaks about *fozen-in magnetic flux* and Equation 2.13 reduces to

$$\frac{\partial \mathbf{B}}{\partial t} = \nabla \times (\mathbf{v} \times \mathbf{B}) \tag{2.15}$$

This equation is identical with the equation for the vorticity in the theory of non-viscous fluids, and is interpreted as implying that any vortex lines move with the fluid. In fact, in can be shown that Equation 2.15 implies that the total magnetic induction encircles by a closed loop remains unchanged even if each point on this closed loop moves with a different local velocity. The field lines are frozen to the plasma. We will call this identifiable field lines *flux tubes*. Thus a flux tube is a kind of generalized cylinder containing a constant amount of magnetic flux. The frozen-in concept implies that all particles and all magnetic flux contained in a certain flux tube at a certain instant will stay inside the flux tube at all instants, independent from any motion of the flux tube or change in the form of its surface [6].
Due to the analogy with hydrodynamics, Equation 2.15 is usually called *hydromagnetic theorem*, but one also finds the name *frozen-in flux theorem* and Equation 2.15 is represented by its equivalent

$$\mathbf{E} + \mathbf{v} \times \mathbf{B} = 0 \tag{2.16}$$

where we have used Faraday's law. Equation 2.16 shows that electric fields can only result from a Lorentz transformation. Moreover, Equation 2.16 contains another important point. Any component of the electric field parallel to the magnetic field must vanish, due to in an infinitely conducting plasma the cross-product between any velocity component parallel to the magnetic field and the field itself is zero [6].

## The Chapman-Ferraro Magnetosphere

The basic nature of the interaction between the solar wind and the terrestrial magnetic field was first deduced by Chapman and Ferraro. It is based on two theoretical principles [31]:
The first concerns in which way the plasmas interact with the magnetic fields; they behave approximately, as they are "frozen" together. This follows as a consequence of Faraday's law (Equation 2.8), from the fact that in an electrically conducted plasma the electric field in the rest frame is close to zero, otherwise large electric currents would be driven (see above). As a result of this freezing together, magnetic fields are transported by flowing plasmas. For example, if patches of plasma populating different sections of a bundle of field lines move into different directions, the field lines are bent and twisted as the flow bends and twists [31].
The second principle concerns the magnetic field's effect on plasma, due to the Lorentz force $q \cdot (\mathbf{v} \times \mathbf{B})$. Summed over all the charges in a given region, the net force usually resists the bending and twisting, or the compression of the magnetic field lines. There are two components of this force: First, the field exerts an effective pressure on the plasma proportional to the square of the magnetic field. This force resists compressions or attenuations of the magnetic field; Second, bent field lines exert a tension force on the plasma, like that of stretched rubber bands. This force opposes the bending and twisting of the field lines [31].
Applying this ideas of Chapman and Ferraro to the interaction between the solar wind and the Earth, we conclude that since the solar wind plasma is frozen to the IMF, and the Earth's plasma to the Earth's magnetic field, the plasmas will not mix. the solar wind will confine the Earth's field, to a cavity around the planet, forming the magnetosphere (see subsection 2.1.2).

## Magnetic Merging

An important situation where the frozen-in flux concept, at the boundary between two magnetized plasmas, breaks down is the process of *magnetic merging*. Here the magnetic topology changes due to field lines are cut and reconnected to other field

lines. This process in detail is theoretically quit complicated and at the moment poorly understood [9]. Here, we will threat only the basic structure of this process as illustrated in Figure 2.3.

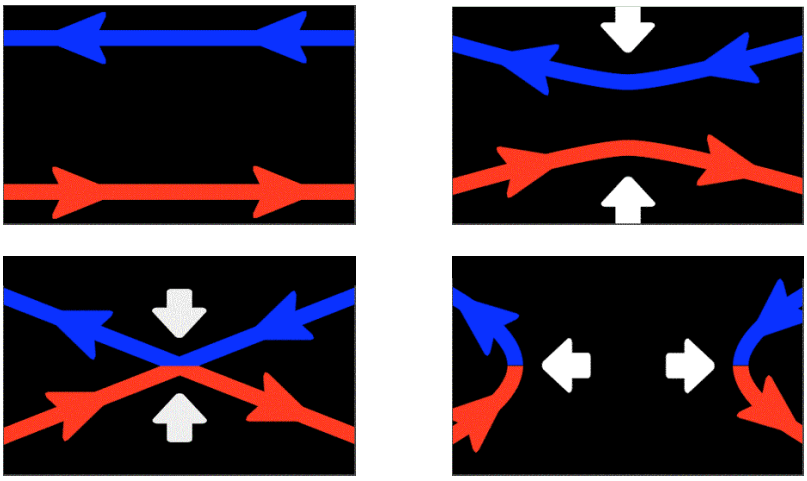

Figure 2.3: Time evolution of field line merging [10].

Consider a magnetic topology with antiparallel field lines frozen into the plasma, like sketched in the upper left panel of Figure 2.3. Such a topology exists around thin current sheets like at the magnetopause and in the tail neutral sheet (see Figure 2.1). If the field lines do not move, such a topology may be stable for a quite long time [6]. However, when plasma and field lines on both sides move toward the currentsheet, sketched in the upper right panel of Figure 2.3, the situation will change.
Due to diffusion at a particular point, the magnetic field may vanish and the laws by which ions and electrons are attached to magnetic field lines break down.This results in the so called *X-type* configuration shown in the lower left panel of Figure 2.3, with the magnetic field being zero at the center of the X, the magnetic *neutral point*. The field lines forming the X and passing though the neutral point are called *separatrix*. [6]. The plasma and field lines are being transported toward the neutral point from either side. at the neutral point the antiparallel field lines are cut into halves and the field line halves from one side are reconnected with those from the other side.
The merged field lines are then in expelled from the neutral point shown in the lower right panel of Figure 2.3. The merged field lines will be populated by a mixture of plasma from both sides of the current sheet. This process continues as long as the oppositely directed flux tubes reject each other and as long as anomalous resistivily [11] lets the magnetic field vanish inside a small volume of space [6].

[9] Interested reader may find the review paper from M. Yamada and H.Ji [18] useful

[10] [Source: http://sci.esa.int]

[11] Due to the *anomalous collisions* of the interaction of the particles with the self generated electric field [6].

## The Dungey's Cycle

In Figure 2.1 the interplanetary field lines (IMF) are compressed against the magnetopause and draped over it by the flow, but ultimately slip around the sides of the magnetosphere, frozen into the magnetosheath plasma [31]. The concurrent drift of the plasma and the field lines as a whole is called *convection*. Because of the infinite conductivity of the plasma, the electric field in the frame of reference moving with the plasma and the flux tubes at velocity $\mathbf{v}_c$ is zero. However, corresponding to the Lorentz transformation, an observer in the Earth's fixed frame of reference will measure an electric field [6] $\mathbf{E}_c = -\mathbf{v}_c \times \mathbf{B}$. So the flow of the plasma and the field lines is associated with a large-scale electric field the so called *convection electric field*. The main source of magneotspheric convection is the momentum of the solar wind flow. The flow of the magnetized solar wind represents an electric field in the Earth's frame of reference. But since the solar wind cannot penetrate the magneotpause (see The Chapman-Ferraro-Magnetosphere), this electric field cannot directly penetrate in the Earth's magnetosphere. However this "frozen-in" picture is only an approximation, and under some circumstances it will break down. Dungey was the first to recognize the importance of this breakdown and study its consequences. One of those circumstances occurs when the IMF has a southward component, the northward directed terrestrial field lines at the dayside magnetopause are allowed to merge with the IMF (see Magnetic Merging). Dungey called this process *magnetic reconnection*

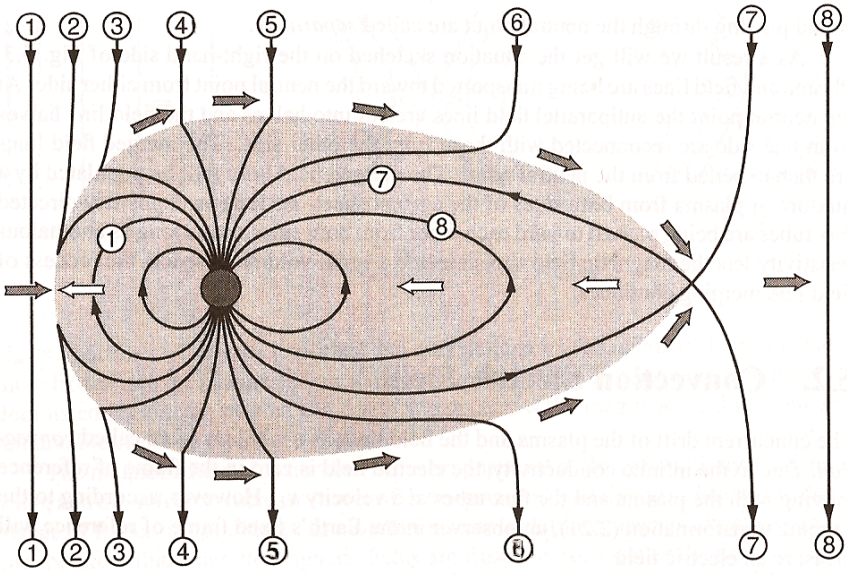


Figure 2.4: Dungey Cycle of reconnection at the magnetopause [12].

[12] [Source: [6]]

In Figure 2.4 the southward directed IMF (denoted by 1) encounters the magnetopause and will merge with the closed terrestrial field line 1. The merged field lines will split into two open field lines marked by 2, each of which has one end connected to the Earth and the other end stretched out into the solar wind. The solar wind will transport this field line towards the nightside across the polar cap (field line marked 3-6) and due to the stiffness of the field line, because of the magnetic tension, the magnetospheric part of the field line will also be transported down-tail (grey shaded area).
At the nigthside end of the magnetosphere, around $100 - 200 R_E$ down-tail, the two open field line halves will meet again and may reconnect, leaving a closed but stretched terrestrial field linein the magnetotail and an open solar wind field line down-tail of the magnetosphere (marked by 7 and 8). Because of the magnetic tension, the stretched tail field line marked by 8 will relax and shorten in the Earthward direction. During this process it transports the plasma to which it is frozen toward the Earth. This is the reason for the Earthward convective flow of the plasma in the magnetotail. Due to equilibrium conditions, the field line will be brought back to the dayside magnetosphere and replace the terrestrial field line denoted by 1 in Figure 2.4, otherwise the dayside of the magnetosphere would soon be devoid of magnetic flux [6].
If the IMF has still a southward component, the same cycle can be repeated. The cycle is referred to by the name *Dungey Cycle*.
However it is important to realize, that the strength of the magnetosphere flow is modulated by variations in the IMF. The dayside reconnection rate, and hence the flux throughput in the magnetosphere, is strong when the IMF points south, opposite to the eqatroial field of the Earth. When the IMF points north, equatorial reconnection cannot occur, and the flow dies away. However, the magnetic flux throughput in the system, even at its strongest, amounts to no more than $\sim 20\%$ of the IMF brought up to the dayside magnetosphere by the solar wind. Most of the IMF is indeed deflected around the magnetosphere as deduced by Chapman and Ferraro [31].

## Magnetospheric Substorms

The variability of the magnetospheric flow which is associated with changes in the IMF has been mentioned above as a key feature. However, observations show that when dayside reconnection is enhanced by a southward turn of the IMF, the magnetosphere generally does not evolve smoothly toward a new steady state of enhanced convection. Instead, the system, especially the tail, undergoes a characteristic evolution on a $1 - 2$ h time scale called a *magnetospheric substorm* [31].
But there is no need for identical instantaneous dayside and nightside reconnection. Actually, it has been found that only part of the flux transported into the tail is reconnected instantaneously and convected back to the dayside. The remaining field lines become added to the tail lobes, where they increase the magnetic flux density. After about one hour these intermediately stored field lines are suddenly reconnected in the tail and their magnetic energy is explosively released [6].

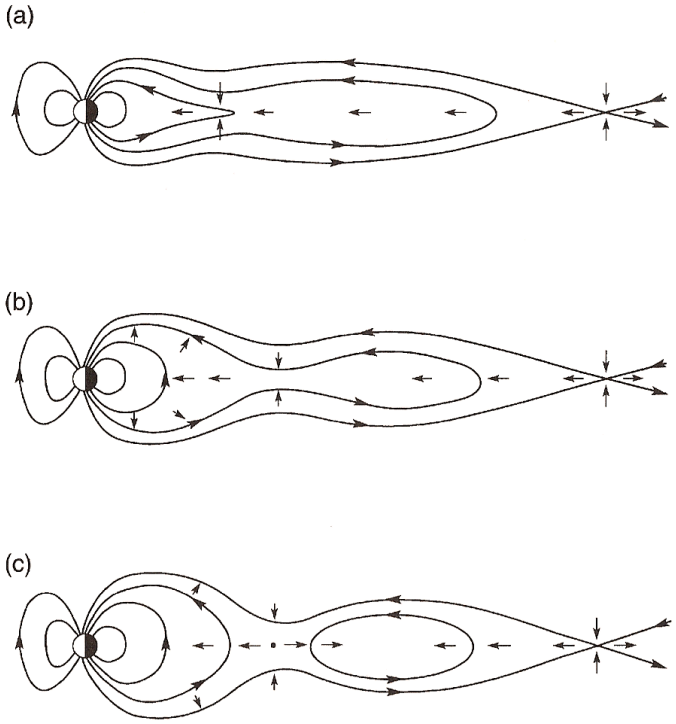


Figure 2.5: Reconfiguration of the plasma sheet during a substorm[13].

**Substorm Growth:** Suppose the magnetosphere is initially in a state of low flow during an interval of nothrward IMF, and that the IMF turns southward. Reconnection starts at the magnetopause, stripping flux from the dayside and transporting it into the tail, so that the dayside magnetopause reduces (by up to $\sim 1R_E$), while in the tail both the radius and the magnetic field strength increase [31]. Since the magnetic field in the tail lobes and the neutral sheet current are related by Bio-Savart's law, the growth of the tail lobe magnetic field must be accompanied by a growing neutral sheet current. The growth of the neutral sheet current will also stretch the field lines threading the plasma sheet into a more tail-like configuration. The plasma sheet becomes concentrated in a layer that is only $500 - 1000$ km thick (Figure 2.5 (a)), compared with quiet-time thickness of $\sim 30000$ km. This thin layer develops in intensity but otherwise remains stable during this initial "growth phase", which lasts tens of minutes [31]. Why this happens is at the moment poorly understood and topic of much research. The period of enhanced convection and loading of the tail with magnetic flux is called *substorm growth phase* [6].

**Substorm Onset and Expansion:** Then on time scales of $\sim 1$ min, the layer disrupts, again for reasons yet to be determined in detail. In principle too much magnetic

[13][Source: [31]]

flux and thus magnetic energy has been accumulated in the tail, so the tail becomes unstable and tries to get rid of the surplus energy. This is the time of *substorm onset* and the beginning of the *substorm expansion phase* [6]. However, the current suddenly decreases and the distended tail-like field lines collapse inward toward the Earth and outward at higher altitudes, to a more dipolar form (Figure 2.5 (b)). As they do so, the plasma they contain is strongly heated and compressed. The collapse usually starts in a restricted longitude sector near midnight in the near-Earth end of the tail (typically at distances of $8 - 20R_E$), and then propagates both down and across the tail [31]. The steched magnetic field in ther plasma sheet becomes more dipolar again, as one can see in Figure 2.5 (b). The elevation angle of the magnetic field in the plasma sheet rises during the substorm expansion. The dipolarization of the magnetotail field is the signature of dramatic reconfiguration of the plasma sheet (see Figure 2.6).

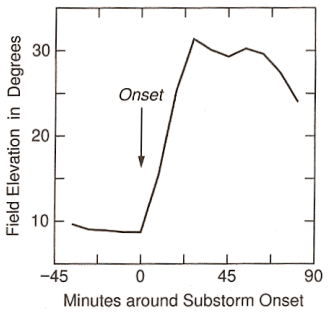


Figure 2.6: Variation of the magnetic field elevation during the substorm[14].

This field collapse often induces the onset of reconnection in the plasma sheet at distances of $20-40R_E$ as propagates down-tail. To distinguish it from the distant neutral line at around $100 - 200R_E$, the newly formed X-line is usually called *near-Earth neutral line*. The large region of the tail between the two neutral lines forms a *plasmoid* (Figure 2.5 (c)). Its field lines are neither connected to the terrestrial nor to the IMF, but form closed loops [6].

**Substorm Recovery:** The subsequent recovery phase typically lasts for many tens of minutes. The strong dipolar field orientation in the tail plasma sheet start to decrease again. In general, reconnection at the near-Earth neutral line ceases and substorm activity settles. This phase ends when the magnetosphere has returned to a quiet state. Besides the general decrease in activity, an important process occurs during the recovery phase. The near-Earth neutral line starts to retreat tailward at the time of maximum expansion. In doing so, it pushes the plasmoid tailward until it is finally ejected from the magnetotail. Its plasma is lost to the

[14] [Source: [6]]

downtail solar wind and the former near-Earth line has become the distant neutral line [6].

### 2.1.5 Theoretical Approaches

The dynamics of a plasma is controlled by the interaction of the charge carriers with the electric and magnetic fields. If all fields were of external origin, the physics would be relative simple. But since the particles move around, their motions may create electric currents and thus magnetic fields. This internal fields and their feedback onto the motion of the plasma charge carriers make plasma physic difficult [6].
In general the dynamics of a plasma can be described by solving the equation of motion for each individual particle. But the electric and magnetic fields in each equations include the internal fields generated by every other moving particle, so all equations a coupled and have to be solved simultaneously. Such a full solution is not only too difficult to obtain, but also of no practical use, since only average quantities like density and temperature are interesting rather than the individual motion of each particle. Therefor, one usually makes certain approximations suitable to the problem studied. It has turned out, that four different approaches are most useful [6]:

1. The simplest approach is the *single particle motion* description. This approach neglects the collective behaviour of a plasma and describes the motion of a particle under the influence of electric and magnetic fields. It is useful to study very low density plasma.
2. The *kinetic theory* is the most developed plasma theory. Instead of solving the equation of motion for each particle, it examines the development of the distribution function for the system of particle in the phase space. Still certain simplifying assumptions have to be made.
3. The *magnetohydrodynamic* approach neglects all single particle aspects and the plasma is treated as a single conducting fluid with macroscopic variables, like average density, velocity and temperature. It assumes that the plasma is able to maintain local equilibria and is suitable to describe the behaviour of a plasma immersed in magnetic (and electric) fields.
4. The *multi-fluid* approach is similar to the magnetohydrodynamic approach, but accounts for different particle species (electrons, protons, and posibly heavier ions) and assumes that each species behaves like a separate fluid. So the different properties of the light electrons and the heavier ions can be taken into account.

However, in this section only the essential basics (which are relevant for chapter 3) of these approaches are described, since a detailed explanation of these theories is to excessive. For further information the reader is recommended to review i.e. the book from [6] W. Baumjohann and R. A. Treumann, *Basic Space Plasma Physics* or in german, the script from [13] M. Heyn, *Teilchendynamik im Plasma*.
In the following we will start with the repetition of the Gyration and the Electic- a. Magnetic Drifts from the single particle approach. Subsequently, we will derive the Vlasov Equation of the kinetic theory, and then turn to the fluid theories and their approaches.

## 1. Single Particle Motion

In a situation where the charged particles do not directly interact with each other and where they do not affect the external magnetic field significantly, the motion of each individual particle can be treated independently. This *single particle approach* is only valid in plasmas where collective effects are negligible and the external magnetic field is rather strong compared to the magnetic field produced by the electric current due to the charged particle motion. However, in order to understand the collective behavior of the plasma, i.e. the motion of the charge carrier under the influence of electric and magnetic fields generated by the motion itself, it is very instructive to study first the motion of charged particles in electric and magnetic fields [6].

### a) Gyration

The equation of motion for a particle of charge $q$ under the action of the Coulomb and Lorentz forces can be written as

$$m\frac{d\mathbf{v}}{dt} = q(\mathbf{E} + \mathbf{v} \times \mathbf{B}) \tag{2.17}$$

where $m$ is the particle mass and $\mathbf{v}$ the particle velocity. If the electric field is absence this equation reduces to the Lorentz force

$$m\frac{d\mathbf{v}}{dt} = q(\mathbf{v} \times \mathbf{B}) \tag{2.18}$$

Taking the dot procuct of this equation with $\mathbf{v}$ and noting that $\mathbf{v} \cdot (\mathbf{v} \times \mathbf{B}) = 0$ (see A.3), the particle kinetic energy as well as the magnitude of its velocity are constans. Thus a static magnetic field does not change the particle kinetic energy.
The direction of the Lorentz force is given by the cross product of the velocity and magnetic field and will always act perpendicular to the direction of motion, causing the particle to move in a circle. The radius of this circle, the so called *gyroradius* $r_g$, can be obtained by equating the Lorentz force to the centripetal force:

$$qv_\perp B = \frac{mv_\perp^2}{r_g} \tag{2.19}$$

where $v_\perp = (v_x^2 + v_y^2)$ is the constant velocity in the plane perpendicular to the magnetic field. Thus, the *gyroradius* is determined to be:

$$\boxed{r_g = \frac{mv_\perp}{qB}} \tag{2.20}$$

and is directly proportional to the particle mass and velocity, and inversely proportional to the particle electric charge, and the magnetic field strength.

Solving the Equation 2.19 for the velocity $v_\perp$ and since $v/r$ is equal to the angular velocity $\omega$, we get

$$\boxed{\omega_g = \frac{qB}{m}} \tag{2.21}$$

where $\omega_g$ is the *gyrofrequency* or *cyclotron frequency*.

### b) Guiding Center Drifts

Since the Lorentz force is always perpendicular to the magnetic field, it has no influence on the parallel motion. In a uniform field with no additional forces, a charged particle will gyrate around the magnetic field according to the perpendicular component of its velocity and drift parallel to the field according to its initial parallel velocity, resulting in a helical orbit. However, when there is a force on the particles perpendicular to the magnetic field, it will result in superimposition of a relatively fast gyratory motion around a point called the *guiding center* and a relatively slow drift of this point.

#### General Force Drift

To derive a general form of guiding center drift under a force $\mathbf{F}$, which is valid not only for the Coulomb force, but for any force acting on a charged particle in a magnetic field, we assume that the transformed velocity $\mathbf{w}$ in a new frame of reference is only a gyratory motion

$$\mathbf{v} = \mathbf{w} + \frac{\mathbf{F} \times \mathbf{B}}{qB^2} \tag{2.22}$$

If the general force $\mathbf{F}$ is perpendicular to the magnetic field $\mathbf{B}$

$$\begin{aligned} m\dot{\mathbf{w}} = m\dot{\mathbf{v}} &= \mathbf{F} + q(\mathbf{v} \times \mathbf{B}) \\ &= \mathbf{F} + q\mathbf{w} \times \mathbf{B} + \frac{(\mathbf{F} \times \mathbf{B}) \times \mathbf{B}}{B^2} \\ &= \mathbf{F} + q\mathbf{w} \times \mathbf{B} - \frac{B^2\mathbf{F}}{B^2} \\ &= q\mathbf{w} \times \mathbf{B} \end{aligned}$$

As one can see the result is a gyratory motion in the new frame of reference. Therefore, the equation for the general force dirft velocity of the guiding center is

$$\boxed{\mathbf{v}_F = \frac{\mathbf{F} \times \mathbf{B}}{qB^2} = \frac{1}{\omega_g}\left(\frac{\mathbf{F}}{m} \times \frac{\mathbf{B}}{B}\right)} \tag{2.23}$$

All particles drifts can be described this way by using the appropriate force terms, whenever the drift velocity of the particle is much smaller than its gyrovelocity. The obvious case are electric forces (see below Electric Drift). The grad-B drift can be considered to result from the force on a magnetic dipole in a field gradient (see below Magnetic Drift). The curvature (see below Magnetic Drift) and polarisation

drifts (see below Electric Drift) result from treating the acceleration of the particle as fictitious forces. The diamagnetic drift is actually not a guiding center drifts (see (c) Magnetohydrodynamics in this section), but can be derived from the force due to a pressure gradient. Finally, other forces such as radiation pressure and collisions also result in drifts but are not necessary for this master thesis.

**Electric Drift**

The exact nature of the *electric drift* depends on weather the field is electrostatic or time-varying and whether it is spatially uniform or not.

**E×B Drift**

Let us now assume that an electrostatic field, **E**, is present. Looking for solutions of Equation 2.17, we can treat the perpendicular and parallel component to **B** separately. The parallel component describes a straightforward acceleration along the magnetic field line. However, in geophysical plasmas most parallel electric fields cannot be sustained, since they are immediately cancelled out by electrons, which are under most circumstances extremely mobile along the magnetic field lines [6].

Taking Equation 2.23 with the Coulomb force $\mathbf{F} = q\mathbf{E}$, we obtain

$$\boxed{\mathbf{v}_E = \frac{\mathbf{E} \times \mathbf{B}}{qB^2}} \tag{2.24}$$

the general form of the *E×B drift*. The E×B drift is independent of the sign of the charge and thus electrons and ions move into the same direction, so there is no net current (assuming quasineutrality). It is insturctive to note that the E×B drift can be viewed as a result of the Lorentz transformation, so that in the frame of reference moving with the velocity of the particle the electric field vanishes.

**Polarization Drift**

A time-varying electric field results in a *polarization drift* given by

$$\boxed{\mathbf{v}_P = \frac{m}{qB^2}\frac{d\mathbf{E}_\perp}{dt} = \frac{1}{\omega_g B}\frac{d\mathbf{E}_\perp}{dt}} \tag{2.25}$$

where we used for the general force of Equation 2.23 $\mathbf{F}_P = -m\frac{d\mathbf{E}}{dt}$. Obviously this drift is different from the E×B drift in that it depend on the charge and mass of the particle. Thus the polarization drift increases proportional to the mass of the particle. It is directed along the electric field, but oppositely for electrons and ions. Accordingly, it creates a current which carries electrons and ions into opposite directions and polarizes the plasma, hence the name *polarization drift*.

### Magnetic Drift

When analyzing Equation 2.18, we have assumed that the magnetic field is homogeneous. This is often not the case. A typical magnetic field has gradients and often are curved. This inhomogeneity of the magnetic field leads to a *magnetic drift* of charged particles. Time variations on the other hand cannot impart energy to a particle, since the Lorentz force is always perpendicular to the velocity of the particle. However, since $\partial \mathbf{B}/\partial t = -\nabla \times \mathbf{E}$, the associated inhomogeneous electric field may accelerate the particles in the way described above [6].

#### Gradient Drift

Let us now assume that the magnetic field is weakly inhomogeneous. When a particle moves into a larger magnetic field, the gyroradius of the particle decreases and thus the gqroradius of the particle will be larger at the low magnetic field strength. As a result, ions and electrons drift into opposite directions, perpendicular to both $\mathbf{B}$ and $\nabla\ \mathbf{B}$. The drift velocity is

$$\boxed{\mathbf{v}_\nabla = \frac{\mu}{qB^2}(\mathbf{B} \times \nabla B)} \tag{2.26}$$

where we used for the general force of Equation 2.23, $\mathbf{F}_\nabla = -\mu \nabla B$. $\mu$ is the *magnetic moment*

$$\mu = \frac{mv_\perp^2}{2B} = \frac{W_\perp}{B} \tag{2.27}$$

to describe the ratio of the perpendicular particle energy and magnetic field.

#### Curvature Drift

The gradient drift is only one component of the particle drift in an inhomogeneous magnetic field. when the field lines are curved, a *curvature drift* appears. Due to their parallel velocity the particles experience a centrifugal force

$$\mathbf{F}_R = mv_\parallel^2 \frac{\mathbf{R}_c}{R_c^2} \tag{2.28}$$

where $\mathbf{R}_c$ is the local radius of curvature. Inserting this force into Equation 2.23 yields directly the *curvature drift* velocity

$$\boxed{\mathbf{v}_R = \frac{mv_\parallel^2}{q} \frac{\mathbf{R}_c \times \mathbf{B}}{R_c^2 B^2}} \tag{2.29}$$

The curvature drift is proportional to the parallel particle energy, and perpendicular to the magnetic field and its curvature [6].
It should be mentioned that in a cylindrically symmetric field (valid in the limit of small plasma pressure), it turns out that $-\nabla B = (B/R_c^2)\mathbf{R}_c$. Thus we may add the gradient to the curvature drift to obtain the total magnetic drift [6]

$$\boxed{\mathbf{v}_B = \mathbf{v}_R + \mathbf{v}_\nabla = (v_\parallel^2 + \frac{1}{2}v_\perp^2)\frac{\mathbf{B} \times \nabla B}{\omega_g B^2}} \tag{2.30}$$

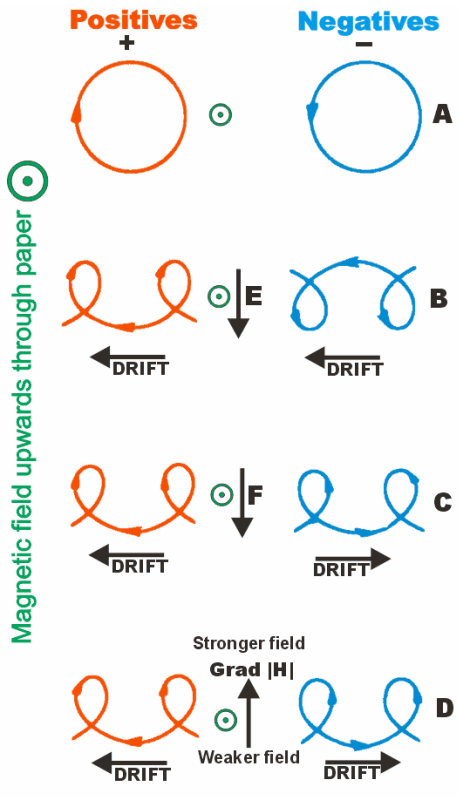


Figure 2.7: Charged particle drifts in a homegenous magnetic field. (A) No disturbing force; (B) With an electric field E; (C) With an independent force F; (D) In an inhomgeneous magnetic field, grad H [16].

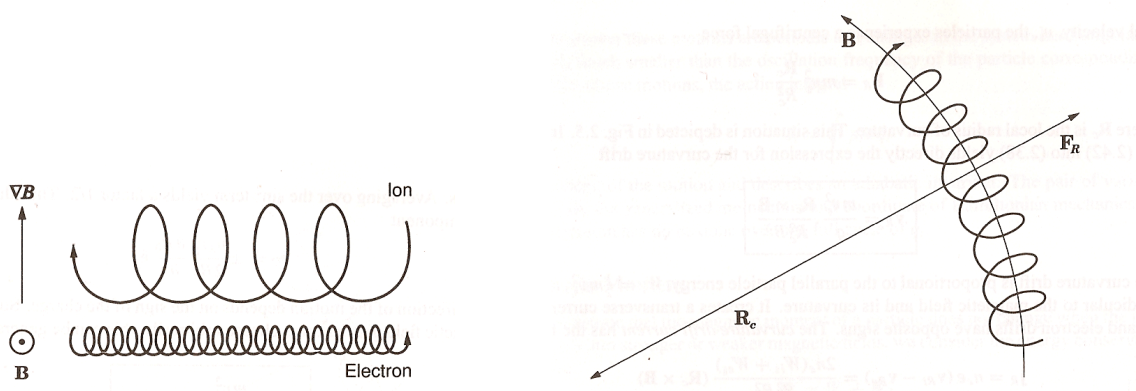


Figure 2.8: Particle drift due to a magnetic field gradient (left) and Centrifugal force felt by a particle along a curved field line (right). [18].

[16] [Source: http://en.wikipedia.org/wiki/Guiding_center]
[18] [Source:[6]]

# 2. Kinetic Plasma Theory

The many-particle character of plasmas leads to a collective behavior, due to a long-range interparticle interactions between the charged particles takes place. A charge carrier is due to the electric fields, **E(x**,t), connected to each point charge, $q$, and the magnetic fields, **B(x**,t), generated when the charges move at a given velocity, **v**. Other charge carriers in the plasma respond to these fields, which leads to momentum and energy exchange between the particles and the fields. As a consequence the actual field configuration is the sum over all the microscopic contributions of the particles to the fields, so the accounting for the full particle dynamics is a very complex and complicated task [6].
One possible way to obtain the field and particle configurations is to consider all the self-generated microscopic fields, to calculate the trajectories of all particles in these fields and to self-consistently account for their self-gnerated fields during this motion. Apparently this leads to enormous computational difficulties. Hence, a statistical description is used, the so called *kinetic plasma theory* [6].
In the followin we will derive the *Vlasov equation*, which may be used to describe the dynamics of a system of charged particles interacting with an electromagnetic field.

## a) Exact Phase Space Density

In contrast to the previous section, where the plasma consisted of single particles, we now assume that there is a strongly interaction between the many particles. Each particle has a time dependent position $\mathbf{x}_i(t)$ and velocity $\mathbf{v}_i(t)$. This two independent coordinates span a six-dimensional space with the axes (**x**,**y**), called the *phase space*. The particle at a certain time $t_0$ is characterized as one point in this space inside a phase space volume element, $d\mathbf{x}d\mathbf{v}$, and the particle trajectory at later times $t$ is a curve in this phase space [6]. The exact number density $\mathcal{F}_i$ of the $i$-the particle is

$$\mathcal{F}_i(\mathbf{x}, \mathbf{v}, t) = \delta(\mathbf{x} - \mathbf{x}_i(t))\delta(\mathbf{v} - \mathbf{v}_i(t)) \tag{2.31}$$

where $\delta$ is the Dirac delta function. The particle density in phase space is different from zero only at the position and velocity of the $i$-the particle at time t. The total exact *particle density* of the plasma is then the sum over all the single particle densities

$$\mathcal{F}(\mathbf{x}, \mathbf{v}, t) = \sum_i \delta(\mathbf{x} - \mathbf{x}_i(t))\delta(\mathbf{v} - \mathbf{v}_i(t)) \tag{2.32}$$

Because the particles building up the phase space volume of the plasma are subject to forces, and the forces are different for each of the particles, the phase space volume of the plasma will deform. However, the number of particles inside the phase space volume does not change, as *Liouville*[19] showed, and the volume remains constant but

[19] The Liouville theorem said that a phase space volume element moves under teh action of the Lorentz force like an incompressible fluid in phase space, because $\nabla \cdot \mathbf{v} = 0$ holds for the phase space coordinates [6].

merely changes its shape.

**Equation of Motion**

The position of the particle is determined by its equation of motion under the action of all microscopic electromagnetic fields. Denoting the microscopic fields by the index $m$, the *equation of motion* is

$$\frac{d}{dt}\mathbf{v}_i(t) = \frac{q}{m}[\mathbf{E}_m(\mathbf{x}_i(t), t) + \mathbf{v}_i(t) \times \mathbf{B}_m(\mathbf{x}_i(t), t)] \tag{2.33}$$

The microscopic electric and magnetic fields are defined as the fields generated by all the particles in the plasma at the exact instantaneous position and satisfy the microscopic *Maxwell equations*

$$\nabla \times \mathbf{B}_m(\mathbf{x}, t) = \mu_0 \mathbf{j}_m(\mathbf{x}, t) + \varepsilon_0 \mu_0 \frac{\partial}{\partial t}\mathbf{E}_m(\mathbf{x}, t) \tag{2.34}$$

$$\nabla \times \mathbf{E}_m(\mathbf{x}, t) = -\frac{\partial}{\partial t}\mathbf{B}_m(\mathbf{x}, t) \tag{2.35}$$

$$\nabla \cdot \mathbf{E}_m(\mathbf{x}, t) = \frac{1}{\varepsilon_0}\rho_m(\mathbf{x}, t) \tag{2.36}$$

$$\nabla \cdot \mathbf{B}_m(\mathbf{x}, t) = 0 \tag{2.37}$$

where $\rho_m$ is the microscopic electric space charge and $\mathbf{j}_m$ the current densities of all particles, which generate the electric and magnetic fields $\mathbf{E}_m$ and $\mathbf{B}_m$. The charge and current densities are defined as

$$\rho_m(\mathbf{x}, t) = \sum_s q_s \int \mathcal{F}_s(\mathbf{x}, \mathbf{v}, t) d^3v \tag{2.38}$$

$$\mathbf{j}_m(\mathbf{x}, t) = \sum_s q_s \int \mathcal{F}_s(\mathbf{x}, \mathbf{v}, t) \mathbf{v} d\mathbf{v} \tag{2.39}$$

where the sum over all particle species $s$ (electrons, protons and heavier ions), with the exact phase space density $\mathcal{F}_s$ and charges $q_s$ has to be taken.
These equations describe the plasma configuration in a exact and self-consistent way. Computer simulations of plasmas can be based on these equations, but due to the large particle numbers such calculations require immense amounts of computer cache memory and hence in most cases unresolvable .

**Klimontovich Dupree Equation**

If no particle is lost from or added to the plasma, the exact phase space density is conserved during the dynamic evolution of the plasma. Thus the total time derivative of $\mathcal{F}(\mathbf{x}, \mathbf{v}, t)$ must vanish

$$\frac{d}{dt}\mathcal{F}(\mathbf{x}, \mathbf{v}, t) = 0 \tag{2.40}$$

The total time derivative in six-dimesional phase space, with the use of the differential chain rule due to the time-dependence of $\mathbf{x}$ and $\mathbf{x}$, is

$$\frac{d}{dt} = \frac{\partial}{\partial t} + \mathbf{v} \cdot \nabla_{\mathrm{x}} + \frac{d\mathbf{v}}{dt} \cdot \nabla_{\mathrm{v}}$$

Using the equation of motion (Equation 2.33) to replace the derivative of the velocity, we obtain

$$\boxed{\frac{\partial \mathcal{F}}{\partial t} + \mathbf{v} \cdot \nabla_{\mathrm{x}} \mathcal{F} + \frac{q}{m}(\mathbf{E}_m + \mathbf{v} \times \mathbf{B}_m) \cdot \nabla \mathcal{F} = 0} \tag{2.41}$$

the *Klimontovich-Dupree equation*, which describes the plasma states in the phase space at all times [6].

### b) Average Distribution Function

Since the Klimotovich-Dupree equation still contains the exact microscopic fields it is difficult to solve. A possible way to ease this, is by averaging over a large number of particles, which suppose to be statistically correlated in time, space and velocity by their mutual interactions [6].

#### Kinetic Equation

We define an ensemble *average phase space density*, $\langle \mathcal{F}(\mathbf{x}, \mathbf{v}, t) \rangle = f(\mathbf{x}, \mathbf{v}, t)$, and express the exact phase space density as the sum of its average and fluctuation, $\delta\mathcal{F}$,

$$\mathcal{F}(\mathbf{x}, \mathbf{x}, t) = f(\mathbf{x}, \mathbf{v}, t) + \delta\mathcal{F}(\mathbf{x}, \mathbf{v}, t) \tag{2.42}$$

Since the fluctuations form a statistically ensemble, the average over the fluctuation vanishes.
In a similar way we compose the electric and magnetic fields

$$\mathbf{E}_m(\mathbf{x}, \mathbf{v}, t) = \mathbf{E}(\mathbf{x}, \mathbf{v}, t) + \delta\mathbf{E}(\mathbf{x}, \mathbf{v}, t) \tag{2.43}$$

$$\mathbf{B}_m(\mathbf{x}, \mathbf{v}, t) = \mathbf{B}(\mathbf{x}, \mathbf{v}, t) + \delta\mathbf{B}(\mathbf{x}, \mathbf{v}, t) \tag{2.44}$$

Inserting these equation into Equation 2.41 and taking the ensemble average yields to the *kinetic equation* for the average phase space density

$$\boxed{\frac{\partial f}{\partial t} + \mathbf{v} \cdot \nabla_{\mathrm{x}} f + \frac{q}{m}(\mathbf{E} + \mathbf{v} \times \mathbf{B}) \cdot \nabla f = -\frac{q}{m}\langle(\delta\mathbf{E} + \mathbf{v} \times \mathbf{B}) \cdot \nabla_{\mathrm{v}} \delta\mathcal{F}\rangle} \tag{2.45}$$

The advantage of this equation is that both, the average distribution $f(\mathbf{x}, \mathbf{v}, t)$ and the average fields, do not depend any more on the single coordinates of all the singe particles of a species. Due to ensemble average the exact positions of the particles has been smeard out. Hence, a probability to find the ensemble in the interval $\{\mathbf{x}, \mathbf{x} + d\mathbf{x}\}$,$\{\mathbf{v}, \mathbf{v} + d\mathbf{v}\}$ is given. Thus $f(\mathbf{x}, \mathbf{v}, t)$ become a propability distribution

function, and the equation above is the dynamic equation for its evolution under the action of the average fields. The term on the right-handside of this equation contains all the correlations between the fields and particles and therfor its calculation poses a very serious problem [6].

**Boltzmann Equation**

As mentioned above, the term in angular brackets of Equation 2.45, which contains the correlation between fields and particles, is rather hard to estimate. However, one way to simplify the kinetic equation is to neglect the correlations between the fields and to account only for correlations between the particles themselves via collisions [6].
Equation 2.45 turns then into the *Boltzmann equation*

$$\boxed{\frac{\partial f}{\partial t} + \mathbf{v} \cdot \nabla_x f + \frac{q}{m}(\mathbf{E} + \mathbf{v} \times \mathbf{B}) \cdot \nabla f = \left(\frac{\partial f}{\partial t}\right)_c} \tag{2.46}$$

where the term on the right-handside is the time rate of change of $f(\mathbf{x}, (\mathbf{v}, t)$ due to all kinds of collisions.
The functional form of this 'collisions term' depends on the approach and has to be specified. There are plenty of different collisions terms, but the most common are the *Krook collision term*, which account the collisions between the charged particles and neutrals, the*Landau collision integral*, which take the Coulomb collision frequency into account, and the *Fokker-Planck equation*, a rather complicated function of the change of velocity of the particles.

**Vlasov Equation**

Because geophysical plasma are collisonless (except the ionosphere), the collision term in the Botzmann equation can often be completely neglected. So the kinetic equation of a plasma turns into there simplest form, the so called *Valsov equation*

$$\boxed{\frac{\partial f}{\partial t} + \mathbf{v} \cdot \nabla_x f + \frac{q}{m}(\mathbf{E} + \mathbf{v} \times \mathbf{B}) \cdot \nabla_v f = 0} \tag{2.47}$$

The Vlasov equation forms the basic of all kinetic theory in collisionless plasma. Its a highly nonlinear equation in six-dimensional phase space which is very difficult to solve in fully gneratlity. Therefor further approximative methods are made to find solutions under special conditions [6].

**c) Macroscopic Variables**

The six-dimensional distribution function $f(\mathbf{x}, \mathbf{v}, t)$ varies in space, velocity, and time. But, since the macroscopic quantities like, density $n$, bulk flow velocity $\mathbf{v}_b$, pressure $\mathbf{P}$ and average temperature $T$ do not depend on the particle velocities, they can be

obtained by integrating the distribution function over all velocities contributing to it. Indeed, due to this rather simple procedure the macroscopic quantities can be estimated from integrating the distribution function.
The $i$-th *moment* of the distribution function is

$$\mathcal{M}_i(\mathbf{x}, t) = \int f(\mathbf{v}, \mathbf{x}, t)\mathbf{v}^i d^3v \tag{2.48}$$

The first few moments are physically relevant:

**Number Density**
is the zero-order moment

$$\boxed{n = \int f(\mathbf{v} d^3v} \tag{2.49}$$

**Bulk Flow Velocity**
is the first-order moment, and describes the macroscopic flow, which denote the mean velocity of the particle species.

$$\boxed{\mathbf{v}_\mathrm{b} = \frac{1}{n}\int \mathbf{v} f(\mathbf{v})\mathbf{v}^i d^3v} \tag{2.50}$$

**Pressure Tensor**
is the second-order moment, and is defined as the contribution of the fluctuation of the velocities of the ensemble from the mean velocity

$$\boxed{\mathbf{P} = m\int (\mathbf{v} - \mathbf{v}_\mathrm{b})(\mathbf{v} - \mathbf{v}_\mathrm{b}) f(\mathbf{v})\mathbf{v}^i d^3v} \tag{2.51}$$

**Temperature**
can be obtained form the thermal pressure $p = nk_B T$

$$\boxed{T = \frac{m}{3k_B n}\int (\mathbf{v} - \mathbf{v}_\mathrm{b})(\mathbf{v} - \mathbf{v}_\mathrm{b}) f(\mathbf{v})\mathbf{v}^i d^3v} \tag{2.52}$$

This temperature is the *kinetic temperature*, which can be calculated for any distribution function. Hence, this temperature is not consequently the 'true' thermodynamic temperature, since each particle species can have its own distribution function and the plasma do not necessarily have to be in a thermal equilibrium.

# 2. Magnetohydrodynamics

In the kinetic plasma theory it has been shown that distribution functions evolve according to kinetic equations, like i.e. the Vlasov equation for collisionless plasma. In many situations, however, its not necessary to know the exact evolution of the distribution function but it is sufficient to determine the spatial and temporal development of the macroscopic moments of the distribution like the densities, velocities and temperatures. Since the macroscopic moments are quantities which are already familiar from the fluid and gas dynamics, the resulting theory falls into the domain of fluid theories. Hence this theory is called *magnetohydrodynamics* [6].
In the following we are going to discuss the basic conditions for the *validity of magnetohydrodynamics* first before we derive the *multi-fluid equation of motion* and proceeding to the *one-fuid magnetohydrodynamic* approximation to this theory. Then we will specify the *generalized ohm's law* and the *magnetic tension* and *plasma beta* from the one-fluid theory. Finally we will obtain the *diamagnetic drift* in the equilibrium state of fluid plasma.

## a) Validity of Magnetohydrodynamics

The magnetohydrodynamics is already a further approximation to the more general hydrodynamic theory, the multi-fluid theory of plasmas. In the magnetohydrodynamics no distinction is made between the different components of the plasma. This approximation requires that time-scales of variation of fields and fluid have to be longer than the characteristic time-scale of the heaviest particle component. Hence the frequency $\omega$, of any change must be smaller than the *ion cyclotron frequency* $\omega_{gi}$ [6]

$$\omega < \omega_{gi} \tag{2.53}$$

Also the length-scale $L$, where the magnetohydrodynamics is applicable must be longer the *ion gyroradius*

$$L < r_{gi} \tag{2.54}$$

These conditions are derived from the equation of motion of the fluid and are very important and generally used for studying low-frquency phenomena in plasmas.

## b) Multi-Fluid Theory

As mentioned before, the fluid theory is looking for evolution equations for the macroscopic moments, such as density $n_s(\mathbf{x}, t)$, bulk flow velocitiy $\mathbf{v}_s(\mathbf{x}, t)$, pressure tensor $\mathbf{P}_s(\mathbf{x}, t)$ and kinetic temperature $T_s(\mathbf{x}, t)$, of the particle species $s$ in a plasma. The definitions of the moments above (see *kinetic plasma theory*) suggests that the evolution equations can be derived from the Vlasov equation [6].

### Continuity Equation

To obtain the continuity equation of the $s$-component fluid of particles in the plasma, we

take the zero-order moment and integrate the Vlasov equation over the entire velocity space

$$\int \left[ \frac{\partial f_s}{\partial t} + \mathbf{v} \cdot \nabla_x f_s + \frac{q_s}{m_s} (\mathbf{E} + \mathbf{v} \times \mathbf{B}) \cdot \nabla_v f_s \right] d^3v = 0 \tag{2.55}$$

Since the velocity space volume does not depend on time, we can exchange the time derivative with the integral

$$\frac{\partial}{\partial t} \int f_s d^3v = \frac{\partial n_s}{\partial t} \tag{2.56}$$

where we used the zero-order moment. Also the spatial components are independent and therefore can be exchanged

$$\nabla_x \cdot \int \mathbf{v} f_s d^3v = \nabla \cdot (n_s \mathbf{v}_s) \tag{2.57}$$

Finally we consider the last term in the integrated Vlasov equation. Applying $\nabla_v$ to the full integrand $(\mathbf{E} + \mathbf{v} \times \mathbf{B}) f_s$ makes it a total differential. According to the Gauss' theorem, the integration of a total differential gives its values at the boundaries. Since the values at the boundaries in velocity space are at infinity and no particle has infinite speed, the distribution function is zero here, and the integral vanishes. Hence the last integral in the integrated Vlasov equation does not contribute and we obtain the *continuity equation*

$$\boxed{\frac{\partial n_s}{\partial t} + \nabla \cdot (n_s \mathbf{v}_s) = 0} \tag{2.58}$$

That means, that in the absence of any interaction processes which create or annihilate particles of the species $s$, the plasma density is conserved during the motion of the fluid [6].

**Equation of Motion**

Since Equation 2.58 couples the plasma density with to the fluid velocity, another equation is required for the velocity of the plasma. This second fluid equation will be derived in the same way as the continuity equation using instead of a zero-moment a first-order moment treatment of the Valsov equation.

$$\int \mathbf{v} \left[ \frac{\partial f_s}{\partial t} + \mathbf{v} \cdot \nabla_x f_s + \frac{q_s}{m_s} (\mathbf{E} + \mathbf{v} \times \mathbf{B}) \cdot \nabla_v f_s \right] d^3v = 0 \tag{2.59}$$

with the identification of the first term

$$\frac{\partial}{\partial t} \int \mathbf{v} f_s d^3v = \frac{\partial}{\partial t} (n_s, \mathbf{v}_s) \tag{2.60}$$

which is the temporal variation of the flux density of a fluid $s$-component. Also for the second term differentiation and integration can be exchanged, because both are independent. The second term becomes

$$\nabla_x \cdot \int \mathbf{v}\mathbf{v} f_s d^3v = \nabla \cdot (n_s \mathbf{v}_s \mathbf{v}_s) + \frac{1}{m_s} \nabla \cdot \mathbf{P}_s \tag{2.61}$$

where we used for the dyadic form $\mathbf{vv}$,

$$\mathbf{vv} = (\mathbf{v} - \mathbf{v}_s)(\mathbf{v} - \mathbf{v}_s) - \mathbf{v}_s\mathbf{v}_s + \mathbf{v}\mathbf{v}_s + \mathbf{v}_s\mathbf{v} \tag{2.62}$$

and the fluid pressure tensor from Equation 2.51 for the first product on the right-handside of this equation. The second product on the right-handside of this equation gives simply $-n_s\mathbf{v}_s\mathbf{v}_s$, since the fluid bulk velocity $\mathbf{v}_s$ is independent of $\mathbf{v}$.
The last integral of the Vlasov equation can be treated by the same method of applying the operator $\nabla_\mathrm{v}$ to the full integrand and subtract the additional part from the total derivative. Hence, this last integral becomes

$$\int f_s(\nabla_\mathrm{v}\mathbf{v}) \cdot (\mathbf{E} + \mathbf{v} \times \mathbf{B}) d^3v = -n_s(\mathbf{E} + \mathbf{v}_s \times \mathbf{B}) \tag{2.63}$$

The final result, when we add up all non-vanishing integrals, is the *momentum density conservation equation* of the $s$-component fluid of plasma

$$\boxed{\frac{\partial(n_s\mathbf{v}_s)}{\partial t} + \nabla \cdot (n_s\mathbf{v}_s\mathbf{v}_s) + \frac{1}{m_s}\nabla \cdot \mathbf{P}_s - \frac{q_s}{m_s}n_s(\mathbf{E} + \mathbf{v}_s \times \mathbf{B}) = 0} \tag{2.64}$$

This is the equation of motion of the $s$-component fluid plasma. It connects the fluid velocity to the density and the electromagnetic forces acting on the fluid, but not on single particles anymore. The equation is closely related to the Navier-Stokes equation from the conventional hydrodynamics with the additional electromagnetic Lorentz force. The appearance of this force in Equation 2.64 couples on the one hand the charged plasma fluid components together and on the other the plasma fluid to the full set of electromagnetic equations.
However, since in Equation 2.64 a higerh order quantity, the pressure tensor $\mathbf{P}_s$ appears, another equation is needed. This is done by multiplying the Vlasov equation by the second-order dyad $\mathbf{vv}$ and integrating over the velocity space. Its result is the *energy density conservation equation*

$$\frac{3}{2}n_s k_B \left(\frac{\partial T_s}{\partial t} + \mathbf{v}_s \cdot \nabla T_s\right) + p_s \nabla \cdot \mathbf{v}_s = -\nabla \cdot \mathbf{q}_s - (\mathbf{P}'_s \cdot \nabla) \cdot \mathbf{v}_s \tag{2.65}$$

where $T_s$ is the temperature defined in Equation 2.52 and $p_s$ is the scalar pressure, which are related by the ideal gas equation $p_s = n_s k_B T_s$. The quantity $\mathbf{q}_s$, is the heat flux vector and $\mathbf{P}'_s$ denotes the stress tensor part of the full pressure tensor $\mathbf{P}_s$. The stress tensor part describes the *shear stress*. Also this equation contains a new undetermined quantity, the heat flux, a third-order quantity, which can be neglected in most cases.

### c) One-Fluid Theory

Now we assume that the plasma consists of electrons of mass $m_e$, and charge $q_e = -e$, and only one ion component of mass $m_i$, and charge $q_i = e$. The charges and currents are defined by

$$\rho = e(n_i - n_e) \tag{2.66}$$
$$\mathbf{j} = e(n_i\mathbf{v}_i - n_e\mathbf{v}_e) \tag{2.67}$$

Du to *quasineutrality* the electric space charge $\rho = 0$ has to vanish, leading to $n = n_e = n_i$. For a current-free plasma, which is not generally the case, the particle flux densities must be equal $n_i\mathbf{v}_i = n_e\mathbf{v}_e$.
In some situations it is convenient to neglect the difference between the particle species and to consider the plasma as a conducting fluid carrying electric and magnetic fields and currents. The fluid field variables become combinations of the densities and velocities of the single components

$$n = \frac{m_e n_e + m_i n_i}{m_e + m_i} \tag{2.68}$$
$$m = m_e + m_i \tag{2.69}$$
$$\mathbf{v} = \frac{m_i n_i \mathbf{v}_i + m_e n_e \mathbf{v}_e}{m_e n_e + m_i n_i} \tag{2.70}$$

the so called *magnetohydrodynamic equations* of a plasma.
In that order the *continuity equation* for the total fluid is

$$\frac{\partial n}{\partial t} + \nabla \cdot (n\mathbf{v}) = 0 \tag{2.71}$$

which was simple derived by multiplying the two-fluid continuity equation for ions and for electrons, adding the two resulting equation, and making use of the first magneto-hydrodynamic equation from above.
More difficult is the construction of the momentum density conservation equation or *fluid equation of motion*, because of the appearance of the nonlinear terms, $n_s\mathbf{v}_s\mathbf{v}_s$. Here we do not explicitly demonstrate how this equation is derived, however, after some calculation Equation 2.64 from the two-fluid becomes

$$\boxed{\frac{\partial (nm\mathbf{v})}{\partial t} + \nabla \cdot (nm\mathbf{v}\mathbf{v}) = -\nabla \cdot \mathbf{P} + \rho\mathbf{E} + \mathbf{j} \times \mathbf{B}} \tag{2.72}$$

where $\mathbf{P}$ is the total pressure tensor. This is the *momentum conservation equation* in magnetohydrodynamics [6].

### Generalized Ohm's Law

The momentum conservation equation (Equation 2.72) contain a new variable, the electric current density, $\mathbf{j}$. To close the system of equations, one therefore needs an

additional expression for the evolution of $\mathbf{j}$. This equation is the *generalized Ohm's law* of a plasma [6].
Since the derivation of this equation is rather long, only the result is given [20] The generalized Ohm's law of a single-fluid magnetohydrodynamic plasma is given by

$$\boxed{\mathbf{E} + \mathbf{v} \times \mathbf{B} = \eta \mathbf{j} + \frac{1}{ne}\mathbf{j} \times \mathbf{B} - \frac{1}{ne}\nabla \cdot \mathbf{P}_e + \frac{m_e}{ne^2}\frac{\partial \mathbf{j}}{\partial t}} \tag{2.73}$$

where $\eta = m_e \nu_c / ne^2$ is the plasma resistivity, and $\mathbf{P}_e$ is the electron pressure tensor.
One recognizes that this equation is more complicated that the simple Ohm's law used in subsection 2.1.4. In addition to the *resistive term*, $\eta\mathbf{j}$, which contains the anisotropic electron pressure term, a Lorentz force term $\mathbf{j} \times \mathbf{B}$ often called *Hall term*, which even in a collisionless plasma gives rise to contribution transverse to both the current and the magnetic field. The last term on the right-handside is the time variation of the current which can be interpreted as the contribution of electron inertia to the current flow.
In an ideally conducting magnetohydrodynamic fluid with $\eta = 0$ the convective approximation or frozen-in condition (see subsection 2.1.4)

$$\mathbf{E} = -\mathbf{v} \times \mathbf{B} \tag{2.74}$$

requires additional assumptions. Vanishing electron pressure gradients and slow time variations of current density are necessary to neglect the two corresponding terms in the generalized Ohm's law. Neglecting the Lorentz force term is more difficult to justify. We will discuss this separately below (Magnetic Tension and Plasma Beta). Neverless, when the transverse currents are small, the ideal magnetohydrodynamic condition is frequently applied to space plasmas [6].

**Magnetic Tension and Plasma Beta**

The Hall term, $\mathbf{j} \times \mathbf{B}$, appearing in Equation 2.72 and Equation 2.73 introduces a new effect which is specific for magnetohydrodynamics. It is the effect of *magnetic tension* on a conducting magnetohydrodynamic fluid [6].
For slow variations, when the displacement current in the plasma can be neglected, the last Maxwell equation of Table A.3 can be rewritten as

$$\mathbf{j} \times \mathbf{B} = -\frac{1}{\mu_0}\mathbf{B} \times (\nabla \times \mathbf{B}) \tag{2.75}$$

The right-handside of the expression can be written by applying some vector algebra

$$\boxed{\mathbf{j} \times \mathbf{B} = -\nabla(\frac{B^2}{2\mu_0}) + \frac{1}{\mu_0}\nabla \cdot (\mathbf{BB})} \tag{2.76}$$

The first term on the right-handside is the *magnetic pressure*, defined as

$$p_B = \frac{B^2}{2\mu_0} \tag{2.77}$$

[20] Interested reader can find a detailed derivation of the generalized Ohm's law in the book Baumjohann and Treumannn [6].

This pressure simply adds to the thermal pressure of the plasma. The second term is the divergence of a *magnetic stress tensor*. The magnetic field introduces a magnetic stress in the plasma, which contributes to tension and torsion in the plasma. This is a consequence of the vector product of current and magnetic field [6].
The concept of magnetic pressure can also be used to define another useful quantity, the so called *plasma beta* parameter. In an equilibrium, isotropic and quasineutral plasma the total pressure is a constant and one can define the plasma beta as the ratio of thermal and magnetic pressure

$$\boxed{\beta = \frac{2\mu_0 p}{B^2}} \tag{2.78}$$

In the case of anisotropic plasma the pressure splits into parallel and perpendicular components

$$\beta_{\parallel} = \frac{2\mu_0 p_{\parallel}}{B^2} \tag{2.79}$$

$$\beta_{\perp} = \frac{2\mu_0 p_{\perp}}{B^2} \tag{2.80}$$

### c) Sationarity and Equilibria

Stationarity implies absence of any time variations which mathematically means that partial and sometimes even total time derivatives are set to zero. So the state of the plasma persists for a rather long time. Hence the plasma is in an equilibrium state - the *plasma equilibria* [6].

#### Diamagnetic Drift

One conclusion, even for the multi-fluid case, which can be obtained, is the *diamagnetic fluid drift*. Therefor we take the *s*-component fluid momentum conservation equation (Equation 2.64) and assume stationary conditions so that the convective derivative terms can be dropped. Then the fluid equation of motion can be written as

$$q_s n_s(\mathbf{E} + \mathbf{v}_s \times \mathbf{B}) = \nabla \cdot \mathbf{P}_s \tag{2.81}$$

We assume that the pressure tensor, $\mathbf{P}_s$ is anisotropic in the form

$$\mathbf{P}_s = p_{s\perp}\mathbf{I} + (p_{s\parallel} - p_{s\perp}\frac{\mathbf{BB}}{B^2}) \tag{2.82}$$

Then Equation 2.81 turns to

$$q_s n_s(\mathbf{E} + \mathbf{v}_s \times \mathbf{B}) = \nabla p_{s\perp} + \nabla \cdot \left[(p_{s\parallel} - p_{s\perp})\frac{\mathbf{BB}}{B^2}\right] \tag{2.83}$$

Rearranging the different terms and taking the cross-product with $\mathbf{B}/B^2$ leads to

$$\mathbf{v}_s = \frac{\mathbf{E}\times\mathbf{B}}{B^2} + \frac{1}{q_s n_s B^2}\mathbf{B}\times\nabla p_{s\perp} + \frac{1}{q_s n_s B^2}\mathbf{B}\times\nabla\cdot\left[(p_{s\parallel} - p_{s\perp})\frac{\mathbf{BB}}{B^2}\right] \tag{2.84}$$

the stationary drift velocity of the *s*-component fluid of the plasma across the magnetic field.
The first term on the right-handside is the already known $\mathbf{E} \times \mathbf{B}$ drift of the fluid, which is the effect of the Lorentz transformation. The second term describes a drift perpendicular to the magnetic field and the perpendicular pressure $p_{s\perp}$. Since the pressure is a moment of the distribution function and thus an average variable of the plasma, the drift arises due to collective behaviour of the plasma. The third term is only relevant for the anisotropic plasma case. This is a fluid drift velocity which depends on the pressure difference and is non-zero only in a curved magnetic field [6]. However, for isotropic stationary plasma only the second drift term is relevant. Therefor we will specify this term in detail.
Consider a plasma of gyrating particles of one species. All particles gyrate in the same direction around the field. In a homogeneous plasma there would be exactly the same number of particles having exactly same but oppositely directed transverse velocities, due to the displacement by just one gyroradius between the particles across the magnetic field, so that the average velocity would be zero. On the other hand, in a non-uniform plasma, the change in transverse pressure can be either due to a gradient in density or a gradient in transverse temperature [6].

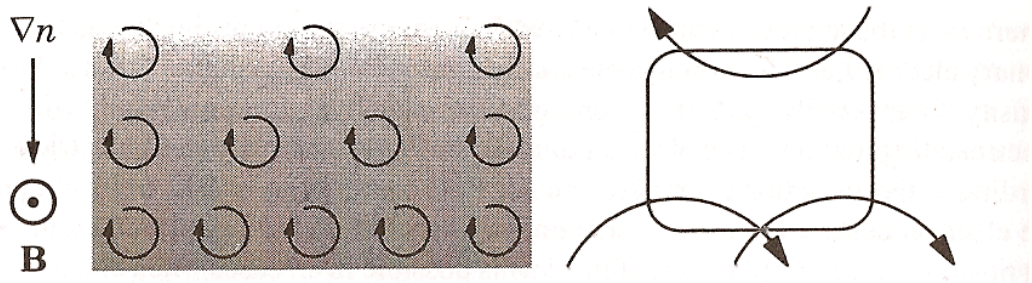


Figure 2.9: Origin of the diamgnetic drift, assuming positive ions. [21].

Due to a transverse density gradient an asymmetry is introduced. Since in the direction of decreasing particle density there are less particle gyrating and, hence, not sufficient oppositely directed velocities to average the transverse velocity out. So there is an excess of transverse particle gyration velocity perpendicular to the density gradient which generate gross fluid drift motion (see Figure 2.9). If the plasma temperature changes across the magnetic field, decreasing temperature implies smaller transverse gyroradii and velocities which are unable to vanish the average velocity [6].
Hence, both temperature and density gradient contribute to a transverse *diamagnetic fluid drift*

$$\boxed{\mathbf{v}_{dia,s} = \frac{\mathbf{B} \times \nabla_{\perp} p_{s\perp}}{q_s n_s B^2}} \tag{2.85}$$

[21] [Source:[6]]

The velocity depends on the charge of the fluid particles, differently charged components will drift into opposite directions, thus an effective drift current flow in the plasma arises. In a quasineutral electron-ion plasma this *diamagnetic current* becomes [6]

$$\boxed{\mathbf{j}_{dia} = \frac{\mathbf{B} \times \nabla_{\perp} p_{\perp}}{B^2}} \tag{2.86}$$

where $p_{\perp} = p_{e\perp} + p_{i\perp}$ is the total perpendicular pressure. The currents are called diamagnetic since they damp the external magnetic field.

## 2.2 Cluster Mission

The **Cluster mission** is an unmanned space mission by the European Space Agency (ESA) to study the small-scale spatial and temporal characteristics of the Earth's magnetosphere. The mission is composed of four identical spacecraft in a tetrahedral formation, which are able to make physical measurements in three dimensions [11].
The Cluster mission was first proposed in 1982 and approved in 1986. Ten years later, 1996, the mission was ready for launch on the first Ariane-5 flight. But, aerodynamic loads on the launcher structure resulted in the breakup of the launcher and the automatic self-destruct system was activated. So the first four Cluster spacecraft were lost, leading to the construction of four new spacecraft. In 2000 the four new Cluster spacecraft "Samba", "Tango", "Rumba" and "Salsa" were successfully launched on Soyuz-Fregat rockets.
Originally the mission was planed to last until the end of 2003, but has been extended several times. Lately the Cluster mission has now been extended until 2012.
This section provides a general overview of the scientific objectives, the configuration and the orbit of the four spacecraft, the Cluster instruments and a short survey of four-spacecraft data analysis techniques.

### 2.2.1 Scientific Objectives

The idea is to investigate the effect of the solar wind on the Earth's magnetosphere in detail. Together with the Solar and Heliospheric Observatory (SOHO) they constitute the Solar Terrestrial Science Programme (STSP), the first 'Cornerstone' of ESA's Horizon 2000 Programme [11].
The main goal of the Cluster mission is to study the small-scale plasma structures in space and time in the key plasma regions (see Figure 2.1):

- solar wind and bow shock
- magnetopause
- polar cusp
- magnetotail
- auroral zone.

Since in this master thesis only physical processes in the region of the magnetotail are significant, we will briefly list some of the scientific questions that the four Cluster spacecraft will answer in this region [22].
As in subsection 2.1.2 mentioned, the magnetotail is characterised by magnetic field lines stretched by the solar wind flow in the anti-sunward direction. The outer region consists of two magnetotail lobes and the inner region of the plasma sheet boundary

[22] More information on the subject can be found in the book *The Cluster and Phonix Missions* from Escoubet et al. [11].

layer and the central plasma sheet (see Figure 2.1). The lobes are large reservoirs of magnetic energy which contain plasma of densities much less than on particle/cm$^{-3}$. A spacecraft in this tenuous plasma will charge to a high positive potentials (up to +50 V). The effect of this potential on low-energy particles measurements is dramatic since the electron measurements are saturated by photo-electrons coming back to the spacecraft and ions are repelled. Therefor the Cluster potential will be controlled by the Active spacecraft Potential Control instrument (ASPOC) and hence will allow measurement of the full distribution functions of the ions and electrons down to around 2 eV. This measurements will determine the role of the lobes as a transient region for the particles originating from the ionosphere and the solar wind. The plasma sheet boundary layer is often the most active plasma region of the magnetotail. Ion beams are observed coming from and toward the Earth. Multi-point measurements are essential to derive the exact origin of these beams and to learn more about the generating mechanism. The Cluster Fluxgate Magenetometer (FGM) is able, for the first time, to calculate the current flowing in the vicinity of the spacecraft without having to make any assumption about the exact shape and orientation of the current sheet. In the centre of the plasma sheet lies the neutral sheet where the magnetic field is weak. The neutral sheet is expected to be the ideal site for magnetic reconnection which accelerates ions toward the Earth and downstream (see subsection 2.1.4). The Cluster Research with Adaptative Particle Imaging Detectors (RAPID) will make multi-point measurements of these accelerated particles and allow to derive the characteristics of the acceleration process. The central plasma sheet is the location of the cross-tail current flowing from dawn to dusk. Sometimes a disruption of this current occurs and part of it is directed toward the ionosphere. This disruption initiates in the near-Earth tail and then propagates further downstream at high speed. Furthermore these disruptions seem to be associated with substorms, one of the most intriguing phenomena in the magnetosphere. Cluster will be able to sense remotely the beginning of the disruption when the spacecraft are in the lobes and then observe the consequences of the disruption further down- or upstream in the plasma sheet [11].
However, there are plenty of other physical processes involved in the interaction between the solar wind and the magnetosphere which can be determined by the Cluster spacecraft. In chapter 3 we will obtain single-spacecraft studies and overall characteristics of fast flows and dipolarization in the magentotail, using observation by Cluster. Then we will use multi-spacecraft analysis to examine the characteristics of the dipolaritzations such as the temporal and spatial scale of the dipolarization front. Finally we will determine the associated currents through the gradients in the magnetic field.

Once again, it should be noted that according to the number of spacecraft, different values can be obtained [11]:

1 spacecraft: can measure a confusing picture of particles and fields. No time or spatial distinction can be made.
2 spacecraft: time- and spacedependent events can be distinguished
3 spacecraft: events can be determined exactly in a plane
4 spacecraft: the rotation, divergence and gradient can be calculated

### 2.2.2 Cluster Instrumentation

The four Cluster spacecraft are identical and each contain 11 instruments, all of identical configuration and measuring at the same time [11]. The instruments have the capability to measure the electric and magnetic field magnitudes and directions and the densities and distribution functions of the electrons and ions. In Table 2.3 the 11 instruments and their measurement are given.

| Acronym | Instrument | Measurement |
|---|---|---|
| FGM | Fluxgate magnetometer | Magentic field **B** magnitude and direction |
| STAFF | spatio-temporal analysis of Field fluctuation experiment | Electric field **E** magnitude and direction |
| EFW | Electric field and wave experiment | Magnetic field **B** magnitude and direction of EM fluctuations, cross correlation of **E** and **B** |
| WHISPER | Waves of high frequency and sounder for probing of electron | In active mode - total electron density $\rho$ in passive mode - neutral plasma waves |
| WBD | Wide band data | Electric field **E** waveforms and spectrograms of terrestrial plasma waves and radio emissions |
| DWP | Digital wave processing experiment | Data manipulation |
| EDI | Electron drift instrument | Electric field **E** magnitude and direction |
| ASPOC | Active spacecraft potential Control | Regulation of spacecraft's electrostatic potential |
| CIS | Cluster Ion spectrometry | Ion times-of-flight (TOFs) and energies from 0 to 40 keV |
| PEACE | Plasma electron and current Experiment | Electron energies form 0.0007 to 30 keV |
| RAPID | research with adaptive particle Imaging detectors | Electron energies from 30 to 1500 keV, energies from 20 to 450 keV |

Table 2.3: Instuments and Measurement on Cluster. [23].

For the Cluster data analysis in chapter 3 we will utilize two of these 11 instruments:

**FGM** The fluxgate magnetometer FGM is designed to provide inter-calibrated measurements of the magnetic field vector at the location of the four Cluster spacecraft. The instrument consists of two tri-axial fluxgate sensors and a failure-tolerant data -processing unit with three different resolutions. The average spacecraft spin resolution (4 s), the normal mode resolution of 32 Hz and the burst mode resolution of 128 Hz. However, for the data analysis in chapter 3 we will use the 5 Hz resolution data prepered by the Cluster Active Archive (CAA) (see subsection 2.2.5). The combined analysis of the data from the four spacecraft will yield parameters such as the current density vector and the geometry and structure of discontinuities like the dipolarization front. FGM provides to all other instruments (except ASPOC) the magnetic-field vector and the event memory trigger which is the time when a given scientific event (e.g. onset of the dipolarization) is occurring [11].

**CIS** The Cluster Ion Spectrometry experiment employs two sensors to obtain the full three-dimensional ion distribution of the major species with a time resolution of one spacecraft spin (4 s) and mass per charge plasma composition. One sensor, the time-of-flight ion Compositon and Distribution Function analyser (CODIF) will measure the distribution of the major ion species from ∼0 to 40 keV/q. CODIF also uses a retarding potential analyser to make more accurate measurements below 15 eV/q. The other sensor, the Hot Ion Analyser (HIA), will measure the distribution of the ions without distinction of mass from ∼ 5 to 32 keV/q. HIA is specifically designed for the highly directinal ion beams ovserved in the solar wind [11]. Hence we will use the CODIF data in chapter 3.

[23] Source: [11]

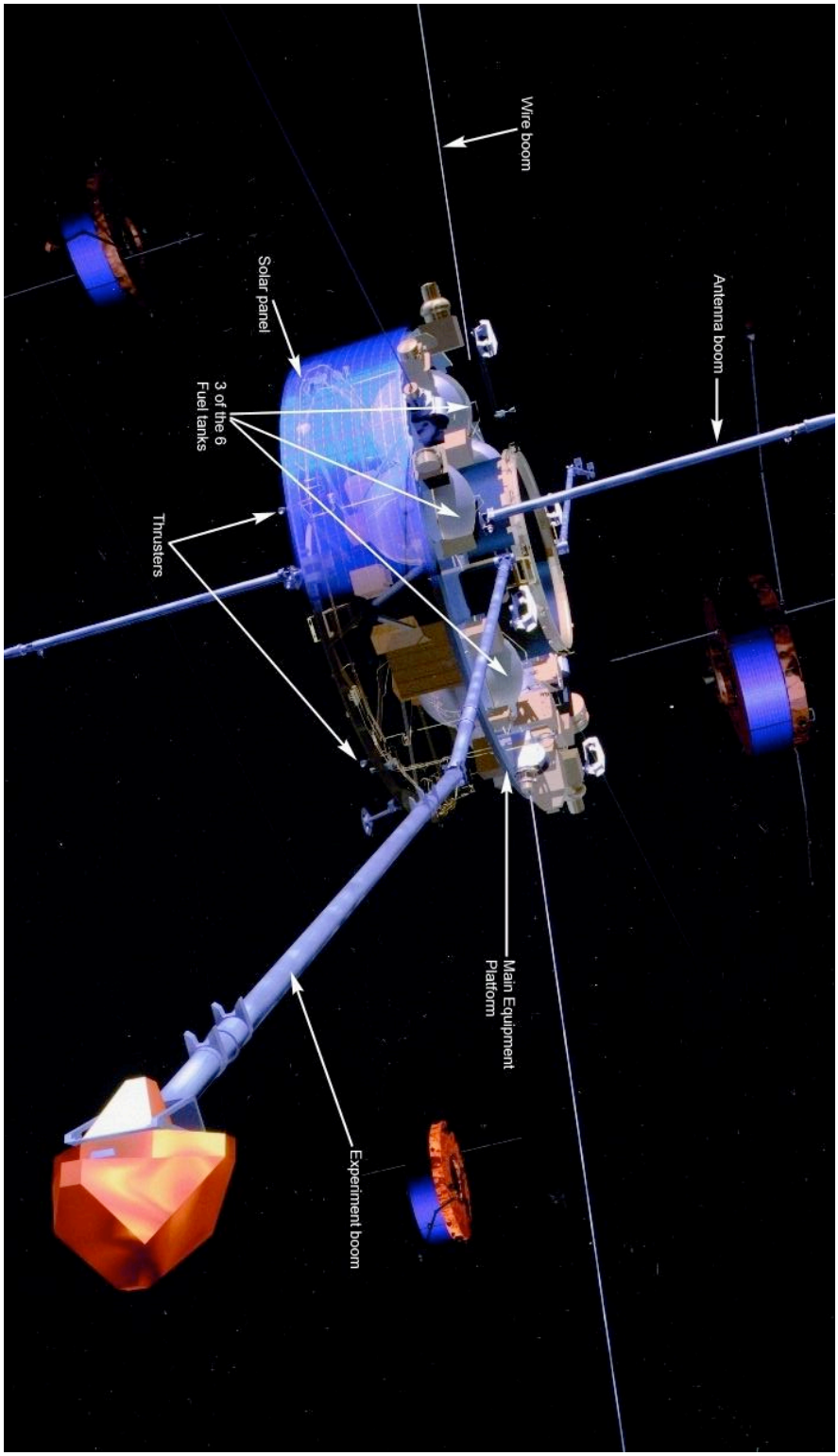


Figure 2.10: Cluster spacecraft. [24].

[24] [Source: http://sci.esa.int/science-e-media/img/d5/hires_36565.JPG]

### 2.2.3 Cluster Orbit and Spacecraft Separation

In order to meet the scientific objectives of the mission, the orbit was chosen with a perigee at 4 $R_E$, an apogee at 19.6 $R_E$, an inclination of 90° and a line of apsides around the ecliptic plane. The mission operation phase started when the spacecraft orbit was in the dawn-dusk meridian with the apogee at dusk (see Figure 2.11). After 3 months, the apogee is in the solar wind around local noon (such orbits occure during the winter season), around the flank of the magnetosphere at dawn after 6 months, in the plasma sheet after 9 months (such jorbits occur during summer season) and then again o the flank of the magnetosphere at dusk on year later. The same scenario will be repeated for the following years of Cluster operations.

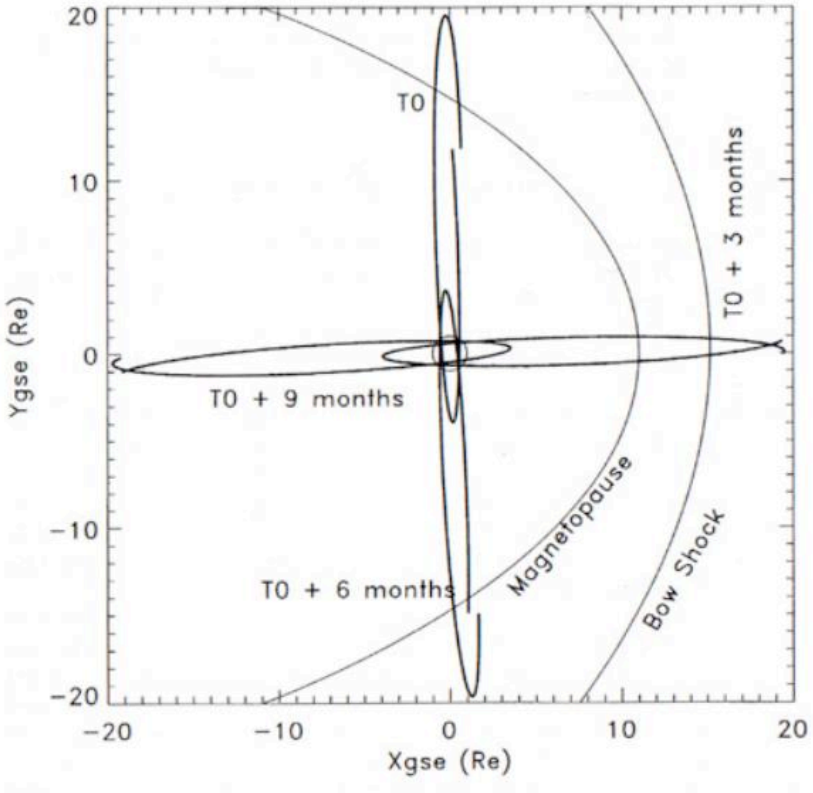


Figure 2.11: Orbits of Cluster spacecraft at three month intervals in the GSE equatorial plane. [26].

A key aspect of the cluster mission is the controllable flight formation. At two locations along the satellite trajectories, the four spacecraft are aligned at the tips of a regular tetrahedron that is the optimal configuration for the measurements of spatial gradients. In other positions the tetrahedron is less regular and near the perigee the satellites fly in a string-of pearls formation, and there are two positions on each orbit where the four satellites are coplanar (see Figure 2.12) [15]. When apogee is in the tail, the regions

[26] [Source: [11]]

crossed by Cluster are the mid-altitude cusp ($\sim$ 4 to 6 $R_E$), the polar cap and tail lobes and the plasma sheet. The spacecraft form a tetrahedron in the plasma sheet. Note, that the spacecraft configuration has been enlarged by a factor of 5 in Figure 2.12 [11]. The size of the tetrahedron formation was changed systematically, covering various distances between 100 and 10000 km during the years 2001-2005. This is necessary to cover the different characteristic spatial and temporal scales of the plasma physics processes. Since 2006, Cluster has been in a multi-scale phase where three satellites fly in a 10000 km trinagular formation and the fourth satellite (Cluster 4) is perpendicular to the plane and is separated from Cluster 3 by a distance varying between 40 km and a few 1000 km [15].

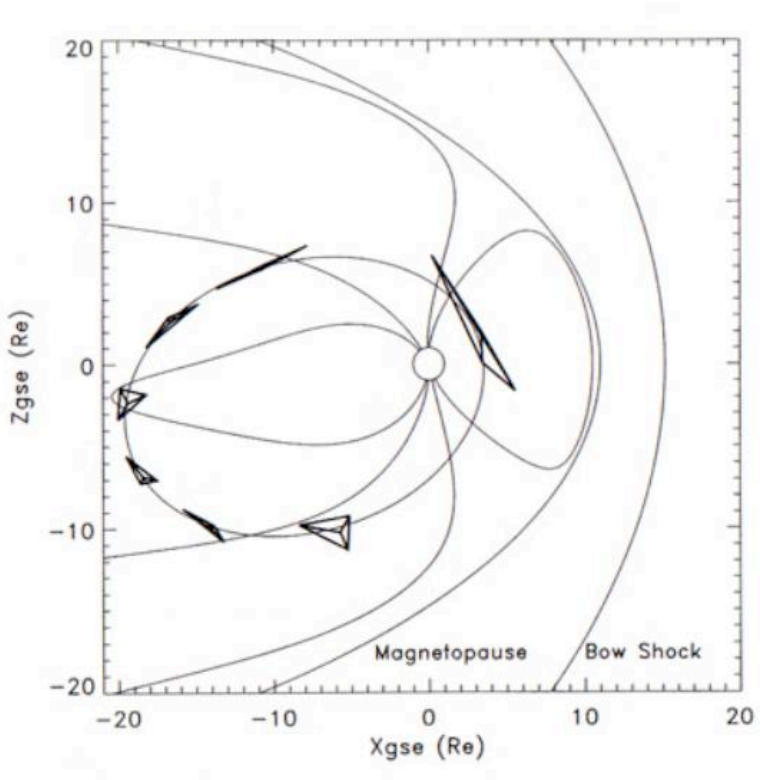


Figure 2.12: Cluster orbit when the perigee is in the solar wind. Such orbits occur during summer season [28].

[28] [Source: [11]]

### 2.2.4 Specific Capabilities of Cluster

Single spacecraft observations can only give limited information on the properties of these observations. One can determine e.g. polarization and use minimum variance analysis to obtain an indication of the propagation direction. However, to obtain more and more accurate information, it is necessary to use multi-spacecraft data. Cluster, with four spacecraft in a tetrahedron configuration, therefor gives the possibility to obtain time series at different locations, which can be used to study the spatial and temporal behaviour of the particles and fields [33].
There are plenty of possibilities to analysis the observations of multiple spacecrafts (e.g. dicontinuity analysis, spatial gradients, k-filtering technique and much more). However, one has to develop the correct analysis technique to extract that extra information. A very useful book in this respect is *Analysis Methods for Multi-Spacecraft Data* from Paschmann and Daly [23]. The main studies which will be performed for the data analysis in chapter 3, are the timing analysis and the curlometer technique. The first part of this subsection is a tutorial-review of the *multi-satellite timing analysis technique* which will be used in section 3.4 to obtain the orientation and motion of dipolarization front. The second part gives an overview of the *curlometer technique* with respect to the barycentre magnetic field, which will be applied in section 3.5 to calculate the diamagnetic current flowing on the dipolarization front.

#### 1. Multi-Satellite Timing Analysis Technique

Harvey [12] introduced a quick and simple method to obtain the orientation and motion of a plane boundary passing by the Cluster spacecraft. We assume that the boundary is propagating with a velocity $\mathbf{v}$ along the normal direction $\hat{\mathbf{n}}$, and that the passing is unambiguously observed by all four spacecraft at $t_\alpha$ with $1 \leq \alpha \leq 4$. These times $t_\alpha$ are assumed to be well determined. In the plane boundary approximation it is evident that only motion in the direction of the normal to the plane can be determined, as any velocity in the plane itself will be indistinguishable, since the plane is invariant under translation in the plane, i.e. there is no structure. Then, projecting the separation distances of the spacecraft $(\mathbf{r}_\alpha - \mathbf{r}_\beta)$ onto the normal $\hat{\mathbf{n}}$ and taking the interval between the crossings $(t_\alpha - t_\beta)$ one can write the following expression [33]:

$$(\mathbf{r}_\alpha - \mathbf{r}_\beta) \cdot \hat{\mathbf{n}} = v(t_\alpha - t_\beta) \tag{2.87}$$

Introducing the vector $\mathbf{m} = \hat{\mathbf{n}}/v$ and taking the three independent combinations of SC1 with the other three SC this equation can be turned into a matrix equation:

$$\mathcal{D}\mathbf{m} = \mathbf{T} \tag{2.88}$$

$$\mathcal{D} = (\mathbf{r}_2 - \mathbf{r}_1, \mathbf{r}_3 - \mathbf{r}_1, \mathbf{r}_4 - \mathbf{r}_1) \tag{2.89}$$

$$\mathbf{T} = (t_2 - t_1, t_3 - t_1, t_4 - t_1) \tag{2.90}$$

where $\mathcal{D}$ is a $3 \times 3$-matrix (not a tensor) and $\mathbf{T}$ is a linear array (not a vector). After inversion, Equation 2.87 gives the solution for $\mathbf{m}$ with the necessary and sufficient

condition that $|\mathcal{D}| \neq 0$ [29]:

$$\boxed{\mathbf{m} = \mathcal{D}^{-1}\mathbf{T}} \tag{2.91}$$

Harvey [12] notes that this method cannot be generalized for more spacecraft. It can also not handle the six possible independent time differences determined form combinating different pairs of the four spacecraft. Therefor he proposes a least squares determination in the case of $N \geq 4$ satellites or combinations. The separation $\mathbf{r}_\alpha$ of the spacecraft is determined with respect to the mesocentre, also called *barycentre*, which is the centre of mass if all spacecraft are identical [33]. Then one finds that:

$$\sum_{\alpha=1}^{N} \mathbf{r}_\alpha = 0 \tag{2.92}$$

and the least squares determination takes the following form of minimizing the sum [30]:

$$S = \sum_{\alpha=1}^{N} [\hat{\mathbf{n}} \cdot \mathbf{r}_\alpha - v(t_\alpha - t_0)]^2 \tag{2.93}$$

where $t_0$ is some reference time. Using again the definition for $\mathbf{m}$ and regular least squares matrix theory one finds:

$$m_l = \frac{1}{N}\left(\sum_{\alpha=1}^{N} t_\alpha r_{\alpha k}\right)\mathcal{R}_{kl}^{-1} \tag{2.94}$$

$$\mathcal{R}_k l = \frac{1}{N}\sum_{\alpha=1}^{N} r_{\alpha k} r_{\alpha l} \tag{2.95}$$

where $\mathcal{R}_{kl}$ determines the so called *volumetric tensor*. It is important to mention that this tensor plays an essential role in the determintation of spatial gradients, but here we will not go into any further detail.
An importatnt note needs to be made here [33]:
The timing method is very sensitive to the resolution of the data. So, one is advised to check the result with that using a higher sampling rate of the data. The error in the timing is, obviously, dependent on the time resolution. Furthermore one should low-pass filter the data to investigate low-frequency phenomena instead of using a lower sampling rate.
For boundary crossing, like e.g. the passing of a dipolarization front, the presupposition that the velocity of the boundary is parallel to the normal is usually justified. However in more general cases, the velocity could be in any direction [33].

[29] This condition is statisfied if, and only if, the four SC are not coplanar.
[30] In chapter 3 we use a computer implementation form of the least squares fit (see section A.5).

## 2. Curlometer Technique

This formalism can be applied to calculate the current density **j** flowing though the Cluster Area and given by the Ampere's law $\nabla \times \mathbf{B} = \mu_0 \mathbf{j}$. By treating this current as constant over the tetrahedral volume formed by the four spacecraft, a difference estimate of $\nabla \times \mathbf{B}$ can be made. This estimate forms the basis of the curlometer analysis technique. In reality, the current will always vary to some degree over the tetrahedron and the best (*a priori*) knowledge of this lies in estimating $\nabla \cdot \mathbf{B}$ under the same assumptions [31]. However, Coeur-Joly *et al.* (1995) calculated $\nabla \times \mathbf{B}$ and $\nabla \cdot \mathbf{B}$ along the orbit of Cluster spacecraft and found that the current density was very accurately estimated all along the orbit except at perigee where the deformation of the tetrahedron is too large. Since the configuration of the four spacecraft is a regular tetrahedron during the summer season (see subsection 2.2.3), the error of the estimated current density in section 3.5 is rather small. It also should be noted, that the curlometer technique can only be applied when the spacecraft separation distances are smaller than the current sheet size [11].

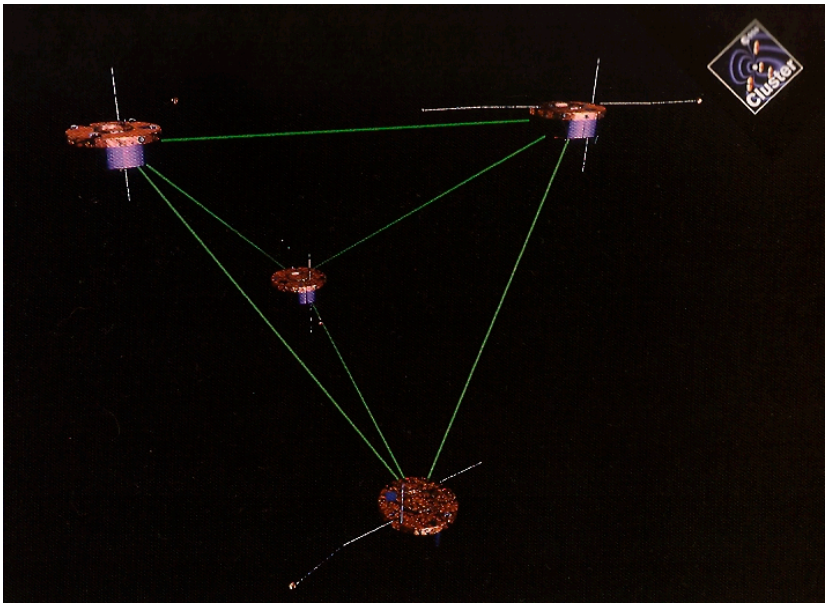


Figure 2.13: The tetrahedral formation of the Cluster spacecraft in orbit [32].

In practice, in section 3.5, we first estimated the Curl of the magnetic field by calculating the gradients of the magnetic fields in the different spacecraft directions. Therefor we obtained the differences between the measured magnetic fields of each spacecraft and multiplied it with the invert of the separation distances of the spacecraft. Then we

[31] For further information the reader is recommended to check section 16.2 of the book *Analysis Methods for Multi-Spacecraft Data* from Paschmann and Daly [23].

[32] [Source: [11]]

calculated the barycentric magnetic field by estimating the gravity centre of the four spacecraft and using the first-order Taylor series approximation with the pre-determined magnetic field gradients. In the next step we obtained the magnetic tension in the field with respect to one spacecraft (e.g. SC 1) which is also the curvature of the magnetic field using the barycentric magnetic fields and the magnetic field gradients. Then a transformation of the magnetic fields in minimum variance coordinates is done to get the minimum variance directions. Finally we determined the current density in minimum variance coordinates by transforming the pre-calculated Curl of the magnetic field in minimum variance coordinates.

### 2.2.5 Cluster Active Archive

The key scientific rationales for the Cluster Active Archive are [15]:

(1) to maximize the scientific return from the Cluster mission by making all high-resolution Cluster data available to the world- wide scientific community
(2) to ensure that the unique Cluster observations are preserved in a stable, long-term archive for scientific analysis beyond the end of the mission
(3) to provide this archive as a major contribution by ESA and the Cluster science community to the International Living With a Star (http://ilwsonline.org/) programme [33]

The Cluster Active Archive (CAA) (http://caa.estec.esa.int) database and services are established and maintained by the ESA at ESTEC in the Netherlands. The CAA aims to provide user-friendly services for searching and accessing these data and ancillary. All data ordered by date, spacecraft, experiment or measurement type. They can be downloaded in a CEF (Cluster Exchange Format) of CDF (Common Data Format) data format. For the data analysis in chapter 3 two types of CAA files (in CDF format) are downloaded:

**CIS-1 (CODIF):** spin-average data (4 s)
Contains the direction and magnitude of the velocity of the ions (typically $H^+$, $He^+$,$He^{++}$ and $O^+$).

**FGM:** spin-average data (4 s) and 5 Hz resolution data
Contains the direction and magnitude of the magnetic field, measured with the Fluxgate Magnetometer. The analysis of data in chapter 3 will be approached two levels. On the first level, we base the selection of events for further analysis on low-resolution data (4s) from one spacecraft (see subsection 3.3.1) and use the so called epoch analysis to conduct a statistical analysis of these events. At the second level, we will use the high-resolution data (5 Hz) of the events because the multipoint analysis is usually very sensitive to the resolution of the data.

All Cluster data are given in the Geocentric Solar Ecliptic (GSE) coordinate system. The GSE system has its $X$-axis pointing from the Earth towards the sun and its $Y$-axis is chosen to be in the ecliptic plane pointing towards dusk (thus opposing planetary motion). Its $Z$-axis is parallel to the ecliptic pole. Relative to an inertial system this system has a yearly rotation.
However, throughout the data analysis in chapter 3 the Geocentric Solar Magnetospheric (GSM) coordinate system is used. The GSM system, as with the GSE systems, has its $X$-axis from the Earth to the Sun. The $Y$-axis is defined to be perpendicular to the Earth's magnetic dipole so that the $XZ$- plane contains the dipole axis. The positive $Z$-axis is chosen to be in the same sense as the northern magnetic pole. The difference between the GSM system and the GSE is simply a rotation about the $X$-axis.

[33] The objective of the ILWS is the study of the Sun-Earth connected system and the effects which influence life and society.

# Chapter 3

# Cluster Data Analysis

## 3.1 Introduction

Magnetotail dipolarizations are usually associated with substorms [e.g. 8], after reconnection has taken place on the stretched field lines, the newly connected field lines will move towards the Earth, releasing the magnetic tension. This creates fast earthward flows [see e.g., 2, 9] and a turning of the magnetic field from the $X$ direction along the tail axis into the $Z$ direction perpendicular to the current sheet in the tail, making it look like a more dipole-like field, hence the name dipolarization.

Note that, although true dipolarization only occurs around geosynchronous distances, this term has been expanded in meaning to include processes that occur in the Earth's magnetotial. In order to keep nomenclature consistent with the many magnetotail papers that have been published over the last years (cited further below) we use terms dipolarization and dipolarization front for the (reconnection) flow-associated magnetic field turnings.

These dipolarizations still leave a lot of questions open, with respect to the details of their structure like: What is the thickness of the dipolarization front, defined as the quick turning from $B_x$ to $B_z$?; Are there currents flowing on the front, and if so, what is the nature of these currents?; Is the structure of the dipolarization front dependent on its velocity?; Why can $B_z$ decrease to become negative before it starts to increase? In this chapter we will try to answer some of these open questions after a short discussion on what has been done before.

Single-spacecraft statistical studies and overall characteristics of fast flows and dipolarizations were obtained, using observations by Geotail [22] and data from Wind [30]. The important characteristics obtained in these two papers for this present study are:

1. The magnetic field becomes dipolar in the course of the fast earthward flow;
2. Sharp dipolarization tends to be preceded by a transient decrease in $B_z$, which

starts along with the fast flow and is accompanied by an increase in the plasma density;

3. The plasma and total pressures decrease in the course of the fast flow.

With multi-spacecraft missions one can better determine the characteristics of the dipolarization front. Sergeev et al. [29] used ISEE 1 and 2 data, measuring a dipolarization of the magnetotail caused by the passage of flux tubes or magnetic bubbles. Nakamura et al. [20] discussed the motion of a diplarization front. It was found that a slow moving front (at $\sim$ 77 km/s) had an estimated size of $\sim$ 2000 km. A study on the propagation of dipolarizations has been done by Takada et al. [32], where both Cluster and Double Star data were used. It was found that flow-associated activity disipates within a limited spatial scale (4 - 8 $R_E$) and that the initial topology of the inner magnetosphere contributes strongly to how far fast flows can penetrate towards the Earth [see e.g., 10].

The THEMIS mission [1], designed to look at the time-history of substorms was used to show the Earthward flowing of a dipolarization front from $\sim$ 20 $R_E$ to $\sim$ 11 $R_E$ at a velocity of $\sim$ 300 km/s. Using the passage-time of the front over the spacecraft it was estimated that the thickness of the front was $\sim 400 - 500$ km, i.e. at the size of the ion inertial length, with the larger size found closer to the Earth [25].

Li et al. [16] studied the force balance around dipolarization fronts within bursty bulk flows by comparing curvature force densities and total pressure gradient force densities ahead of and behind the dipolarization fronts. Indeed plasma acceleration immediatiely after the dipolarization front can be explained by the resultant increased curvature force density.

Dipolarization-associated currents in the magnetotail were studied in a variaty of ways: concerning the substorm current wedge in the near-Earth region [17] and further down the tail [19, 36]. However, determination of the current specifically associated with the dipolarization front has been done by Zhou et al. [38], who found a current layer with a thickness of the ion inertial length. Zahng and V. Angelopoulos [37] studied current carriers observed within thin current sheets ahead of and during the passage of earthward-moving dipolarization fronts in the near-Earth plasma sheet using THEMIS measurements. Contributions by both diamagnetic and polarization currents were found.

However, in this master thesis we will use the data from Cluster and use multi-spacecraft analysis to obtain the characteristics of the dipolarization fronts such as thickness and associated currents. The special set-up of the Cluster spacecraft, i.e. in a tetrahedron-shape in regions of interest (e.g. the magnetotail) gives the possiblity of determining the currents through the gradients in the magnetic field [12].

## 3.2 Data Set and Selection Criteria

For the event selection, we used the 4-sec averaged magnetic field data obtained by the Flux Gate Magnetometer [FGM, 5] and plasma data from the Composition Ion Spectrometer [CIS, 24] on Cluster 1, and throughout the master thesis the Geocentric Solar Magnetospheric (GSM) coordinate system is used. To survey the dipolarization events in the nightside magnetotail, we used the dataset from Cluster between July and October for the years 2001 to 2007, when the spacecraft were located between $-20R_E \leq X_{GSM} \leq -10R_E$ and $|Y_{GSM}| \leq 15R_E$.

To find the dipolarization events, we used similar selection criteria as Takada et al. [32] and Sigsbee et al. [30]. In contrast to these selection criteria we used a 3-min long sliding window instead of a 5-min window. This could result in only "short" dipolarization events, however, it will be shown that there is little effect by the window size. We put on the following requirements on the events:

- The spacecraft is located in the plasma sheet, i.e. plasma-$\beta \geq 0.5$ [7].
- The observed earthward plasma flow (perpendicular velocity $V_\perp$ in $XY$ plane) is at least in one data point (out of 45 data points in the 3-min window) greater than $V_{\perp,x} \geq 150$ km/s.
- The difference in elevation angle $\theta$ between minimum and maximum $B_z$ during the window exceeds $\Delta\theta \geq 10^\circ$ and $\Delta B_z$ also exceeds 4 nT.
- The elevation angle is at least in one data point greater than $\theta \geq 45^\circ$ [8].

We have found 355 dipolarization events using Cluster 1 data. Here we restrict the events for mainly earthward dominant flow. That is, we exclude those events for which the flow turns tailward, faster than -100 km/s within the 3-min window. From the 355 events 219 events were categorized as earthward dominant flow. This means that there is a large percentage (38%) of tailward flows with $V_x < -100$ km/s when one compares this number with what is cited by Angelopoulos et al. [3] for tailward BBFs in the same region (7%). However Angelopoulos et al. [3] set a higher velocity limit for tailward BBFs ($|V| > 400$ km/s). Nakamura et al. [21] found that 22% of the fast flows, with $|V| > 300$ km/s, observed in their study were tailward. From these 219 events 160 events had only positive velocity values and 59 events were categorized as tailward-mixed earthward flow events. That means that these 59 events have a slight tailward flow ($0 > V_{\perp,x} > -100$ km/s) within the 3-min interval. As the majority of flows in the dataset is categorized as earthward dominant flow, only these 219 events will be investigated further.

To maintain that the spacecraft remains near the center of the plasma sheet, close to the neutral sheet, we require additionally: $|B_x| < 5$ nT during the 3-min window. We also set the condition: $|Y_{GSM}| \leq 12R_E$. Consequently 107 events remained for further analysis.

Figure 3.1 shows the positions of Cluster for the 107 dipolarization events in the GSM $XY$ and $YZ$ plane. As stated above, the dipolarization is preceeded by a decrease in $B_z$ and sometimes this decrease is so strong that $B_z$ becomes negative. Out of these 107 events, 69 events had positive minimum $B_z$ values during the dipolarization (marked by circles in Figure 3.1) and 38 events had negative minimum $B_z$ values (marked by stars in Figure 3.1). In the following we examine these 107 events that took place close to the neutral sheet.

## 3.3 Observations

In this section the changes in the magnetic field $B_z$ associated with the plasma flow are investigated. Superposed epoch analyses are conducted, where the median and the upper and lower quartiles are used to get the general shape of the dipolarizations and the variation therein.

### 3.3.1 Event view

Figure 3.2 shows dipolarization events on 29 August 2003 at 1353 UT and 1 October 2003 at 2100 UT. The horizontal axis in Figure 3.2 covers a 2-min interval centered at $t = 0$. This reference time, $t = 0$, corresponds to the start time of the sharpest increase in $B_z$ within the 2-min interval. We will discuss two specific events first, before starting the superposed epoch analysis of all events chosen for this study.

The event on 29 August 2003 (Figure 3.2A) shows a sharp dipolarization front where it took about 4 s to go from $B_{z,min}$ to $B_{z,max}$ (panel D). The magnetic field elevation angle (panel C) to the equatorial plane at Cluster 1 was about $\sim 60°$ before the start of the magnetic dipolarization. There seems to be some oscillations in front of the dipolarization, increasing the elevation angle, after which it decreases to a minimum of $\sim 40°$ at $t = 0$. The elevation angle then increased to a value of $\sim 70°$ at $t = 4$ s and then decreases to $\sim 65°$. The perpendicular plasma flow is shown in panel G. The maximum perpendicular earthward flow in $X$-direction of $\sim 300$ km/s was observed 8 s after the sharp change of $B_z$ and decayed gradually 28 sec after the dipolarization. The plasma flow in $Y$ and $Z$ direction was barely existing.

The event on 1 October 2003 (Figure 3.2B) shows a dipolarization, where it took about 12 sec to go from $B_{z,min}$ to $B_{z,max}$ (panel D). The magnetic field elevation angle to the equatorial plane (panel C) at Cluster 1 was $\sim 50°$. The elevation angle first decreased to a minimum of $\sim -20°$ and then increased back to a value of $\sim 70°$ at $t = 20$ s. The maximum perpendicular earthward flow (panel G) in $X$ direction was $\sim 200$ km/s during the dipolarization. The maximum plasma flow in $Y$ direction was significant higher at $\sim 400$ km/s at the dipolarization and decayed gradually $\sim 20$ s after the dipolarization. The plasma flow in $Z$ direction was negligible.

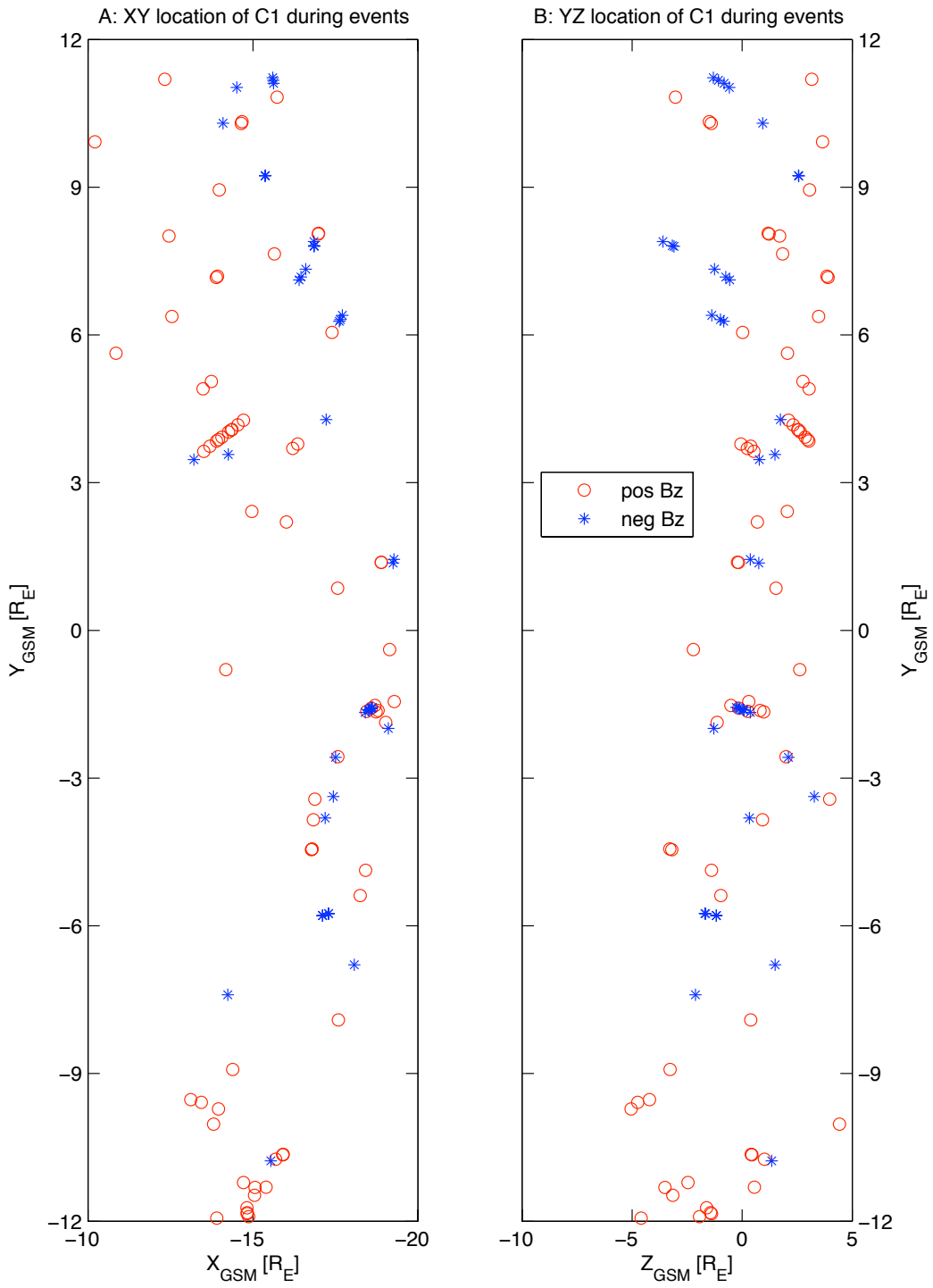


Figure 3.1: Cluster spacecraft position in the $XY$ and $YZ$ plane for the 107 earthward dominant flow events observed during the years 2001-2007. The 69 events with positive minimum $B_z$ values are marked by circles. The 38 events with negative minimum $B_z$ values during the dipolarization are marked by stars.

The plasma-$\beta$, shown in panel A, for both events was 20 and 250 respectively during the dipolarization, indicating that the spacecraft was well situated in the plasma sheet. The increase in plasma-$\beta$ is caused by increasing the plasma density, $N_P$ (shown in panel B), in front of the dipolarization flow due to the compression of the plasma.

Panel H-J in Figure 3.2 shows the electric currents determined by the curlometer technique with the currents perpendicular to the magnetic field (shown as filled region under the red curves). However this will be discussed in section 3.5.

### 3.3.2 Superposed epoch study of dipolarizations

Figure 3.3A shows the $Z$ component of the magnetic field for the 107 dipolarization events ($B_z$, black lines) and the median over plotted ($\overline{B_z}$, red line). The green lines are the upper and lower quartiles of $\overline{B_z}$. As one can see, for the median of all these events the $\overline{B_z}$ drops to a minimum before it starts to increase.

To examine how $B_z$ changes in association with the plasma flow we have divided the dataset into 2 subsets according to the maximum speed of the horizontal perpendicular earthward plasma flow: $150 < V_{\perp,xy} < 400$ km/s and 400 km/s $< V_{\perp,xy}$. These two subsets are studied with a superposed epoch analysis. In Figure 3.3B the relation between the earthward plasma flow velocity $V_{\perp,xy}$ in the horizontal $XY$ plane and the medians of the two superposed $B_z$ is plotted. The result of the superposed epoch analysis shows that the gradient of the dipolarization increases with enhanced velocity. For the low velocity set we find $\Delta B_z \approx 3.5$ nT in $\Delta t = 12$ s, whereas for the high velocity set $\Delta B_z \approx 6$ nT in the same time interval. This observational result suggests that the duration of the dipolarization is anti-correlated with the plasma velocity. Also, the variation in $B_z$ is much greater for the fast flow, a deeper decrease before the dipolarization and a larger end value after the dipolarization. To obtain information about the temporal and spatial scale seperately, it is necessary to use the data not only form Cluster 1 (as up to now) but also from other Cluster spacecraft.

From the 107 dipolarization events, 38 events have an negative $B_{z,min}$ value, see the negative values at $t = 0$ in Figure 3.3A. There can be various possible reasons for a negative $B_{z,min}$ value, with the spacecraft close to the center of the plasma sheet. Amongst possible others, there are:

1. The magnetotail can be tilted in the $YZ$ plane during the observed event and the $B_z$ undershoot becomes negative because of a non-zero $B_y$ component in the tail. In order to test this first explanation, the relation between the mean of the magnetic field in $Y$ direction, $|B_{y,mean}|$ and $Z-$direction, $B_{z,mean}$ of the 38 dipolarization events with a negative $B_{z,min}$ (black circles) is shown in Figure 3.4. The mean average of $B_y$, $B_{y,mean}$ and $B_z$, $B_{z,mean}$ were evaluated during the steady state before the dipolarization occurs.

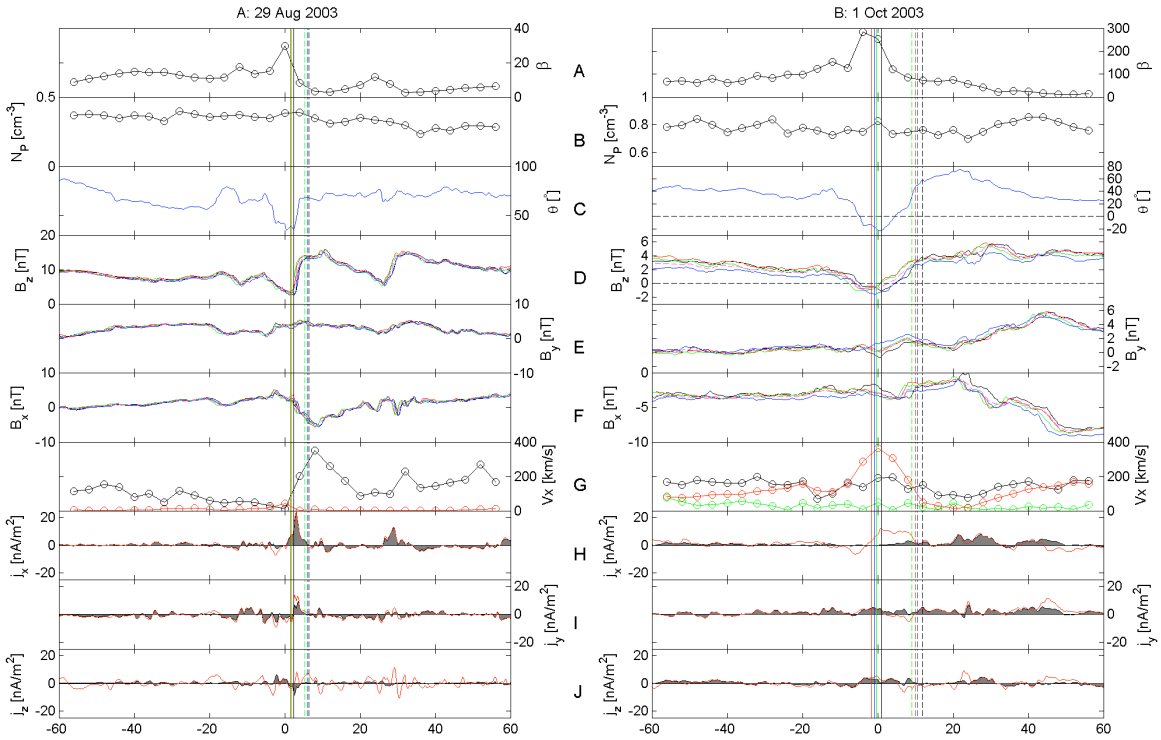


Figure 3.2: Data for 29 August 2003 from 1352 UT till 1354 UT (left panel) and for 1 October 2003 from 2059 UT till 2101 UT (right panel). Panel A: the proton density; Panel B: the plasma-$\beta$; Panel C: the magnetic field inclination angle for C1; Panels D-F: the three magnetic field components for all Cluster spacecraft; Panel G: The perpendicular plasma flow velocity $V_x$ (black), $V_y$ (red) and $V_z$ (green); Panels H-J: The three components of the electric currents determined by the curlometer technique with the current perpendicular to the magnetic field shown as the filled region under the red curves. The two specific times for the 'timing-method' (marked by the horizontal colored solid lines for $B_{z,min}$ and the dashed lines for $B_{z,max}$ are also shown.

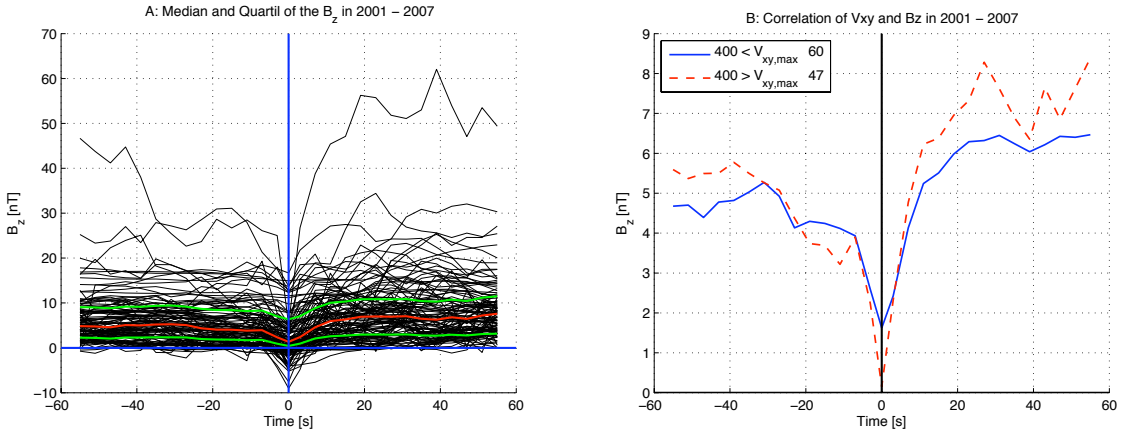


Figure 3.3: The left figure shows the $B_z$ of the 107 dipolarization events (black line) and the median over these events (red line). The green lines are the upper and lower quartile of the median of $B_z$. The right figure shows the relation between the maximum perpendicular plasma flow velocity in $XY$ plane and the median of the superposed $B_z$ for the 107 events. From these 107 events 60 events had a maximum velocity in horizontal $XY$ plane $V_{\perp,xy} < 400$ km/s and 47 events a maximum velocity $V_{\perp,xy} > 400$ km/s during the dipolarization.

2. Strong (diamagnetic) currents on the dipolarization front can generate enough disturbance that $B_z$ can become negative durring the event.

3. A negative $B_{z,min}$ undershoot can also arise from magnetic flux passing over the SC.

4. Transient reconnection is another possible mechanism producing asymmetric bipolar $B_z$ variations, as Kiehas et al. [14] showed.

## 3.4 Multi-Satellite Observations

With the Cluster quartet it is possible to obtain time series at different locations, which can be used to distinguish between the temporal and spatial behavior of the magnetic fields [see e.g., 23, 33]. Harvey [12] showed a simple method to obtain the normal velocity of a plane boundary passing by the Cluster spacecraft, the so called timing-method. Using the spatial configuration of the Cluster spacecraft, one can e.g. cross-correlate the magnetic field data between the spacecraft to obtain the normal velocity of the magnetic structure from which the thickness of the boundary can be inferred.

The timing-method is very sensitive to the resolution of the data. Hence we used 5-Hz resolution data for all 107 dipolarization events which were identified with the 4-sec dataset. The high-resolution data are lowpass-filtered to smooth the data and to conserve the profile of the 4-sec resolution magnetic field data. The best results was

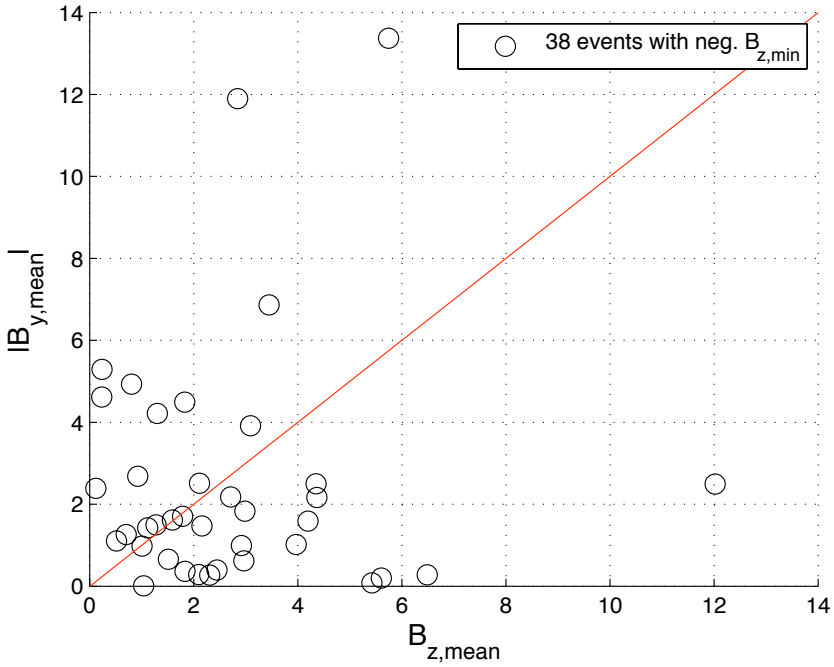


Figure 3.4: The relation between the mean of the magnetic field in $Y$ direction, $|B_{y,mean}|$ and $Z$ direction, $B_{z,mean}$ of the 38 dipolarization events with a negative $B_{z,min}$ (black dots). The mean magnitudes are evaluated during the steady state before the dipolarization is about to occur.

obtained by the use of a lowpass with a cutoff frequency of $f_{cut-off} = 2$ Hz. Indeed the profile of the high-resolution magnetic field data had roughly the same profile as the spin resolution magnetic field data, which means that the "high" frequency noise cannot influence the deformation of $B_{z,min}$ and $B_{z,max}$.

Panels D-F of Figure 3.2 show the magnetic field data of all 4 Cluster spacecraft with 5-Hz data. To obtain the normal velocity of the magnetic structure accurately with the timing-method, we used two specific times (marked by coloured solid lines ('timing' $B_{z,min}$ ) and coloured dashed lines ('timing' $B_{z,max}$) in Figure 3.2B. The particular times are selected automatically by searching the minimum and maximum of $B_z$. Then we estimated the normal velocity of the magnetic structure for each particular time ($V_{timing,min}$ and $V_{timing,max}$). For a first study we are interested in events that are quasi-stationary, i.e. the velocity does not change too much over the structure, and events that show approximately the same profile to limit spatial variations of the dipolarization within the Cluster tetrahedron. In the following we will call these quasi-stationary events "steady" dipolarization events.

The two estimated timing velocities ($V_{timing,min}$ and $V_{timing,max}$) are compared and only events with a velocity difference smaller than 25% are selected, which we will call "steady" dipolarizations. For further analysis the average of these timing velocities ($V_{timing} = (V_{timing,min} + V_{timing,max})/2$) was obtained. From the 107 events 66 remained. Another 42 events had a different profile among the four spacecraft based on visual examination of $B_z$. This indicates that there are, indeed, both temporal and spatial variations in the structures associated with the dipolarizations. Therefore, for only 24 events "steady" structure timing velocity could be found. We also obtained the angle $\alpha$ between the estimated normal velocity of the magnetic structure and the maximum perpendicular plasma flow in $XY$ plane within the 3-min-long time window. From the 24 events 15 events have an angle $\alpha < 90°$ (marked by stars in Figure 3.6) and 9 events have an angle $\alpha > 90°$ (marked by triangles in Figure 3.6). The estimated angle for the event from 29 August 2003 (Figure 3.2A) is $\alpha \approx 30°$ and from the event on 1 October 2003 (Figure 3.2B) $\alpha \approx 150°$. We will discuss the difference between these two flow directions in the discussion section. However, in the following we examine these 24 "steady" dipolarization events.

### 3.4.1 Thickness

The result of the timing-method for the 24 "steady" dipolarization events confirmed the assumption that the temporal duration of the dipolarization is anti-correlated with the horizontal perpendiclular earthward plasma flow velocity $V_{\perp,xy}$ as shown in Figure 3.3. However, there is no systematic behaviour between the thickness of the magnetic boundary $\delta_D$ and the $V_{\perp,xy}$. $\delta_D$ was obtained from the time difference between the minimum of $B_z$ ($t_{timing,min}$) and the maximum of $B_z$ ($t_{timing,max}$), and the estimated average normal velocity of the magnetic structure from the timing-method ($V_{timing}$):

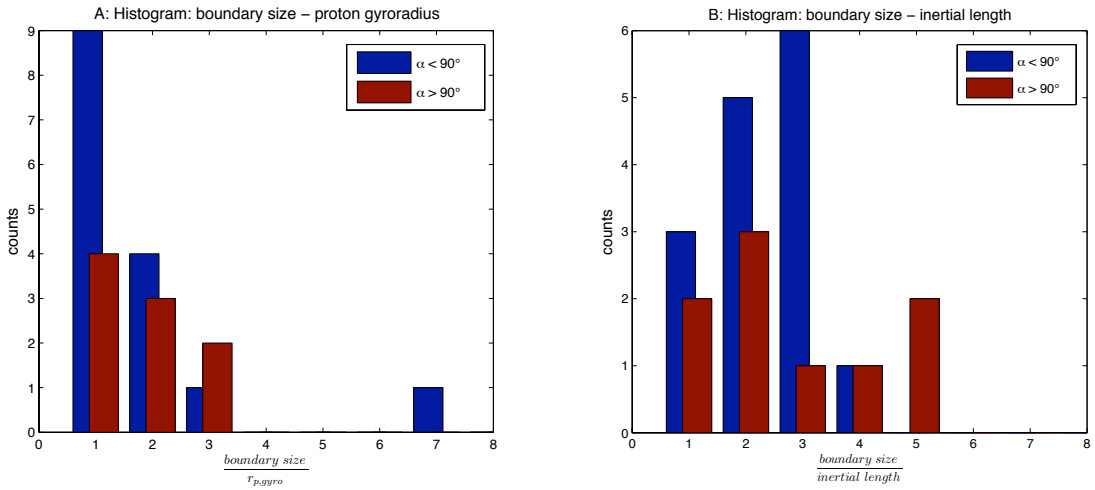


Figure 3.5: The left panel (panel A) shows the histogram of the boundary size normalized by the proton gyro radius of the 24 dipolarization events and the right panel (panel B) shows the the histogram of the boundary size normalized by the ion inertial length. 15 events have an angle $\alpha < 90°$ (marked blue), and 9 events have an angle $\alpha > 90°$ (marked red). The vertical axis in both plots shows the counts normalized with the total number of events of each group.

$\delta_D = (t_{timing,max} - t_{timing,min})V_{timing}$. Like in subsection 3.3.2 we split the data into 2 bins based on the maximum $V_{\perp,xy}$: 150 - 400 km/s and $>$ 400 km/s. From the 24 dipolarization events 11 events have a maximum $V_{\perp,xy} < 400$ km/s and 13 events have a maximum $V_{\perp,xy} > 400$ km/s. The obtained average thickness $\delta_D$ of the dipolarization front is $\sim 460 \pm 350$ km and $\sim 430 \pm 350$ km respectively. So the average size of the boundary ($\sim 450 \pm 350$ km) seems to be independent of the plasma flow velocity and on the order of the evaluated average proton gyro radius of $\sim 590 \pm 150$ km. We also estimated the inertial length of the protons in the magnetic structure: $l_{int} = \omega_p/c \approx 228\sqrt{N_p}$ km, where $\omega_p$ is the plasma frequency, $N_p$ is the proton density in $cm^{-3}$. In additon the relationship between the estimated boundary size and the observed distance from Earth were considered, but no clear correlation was found. Also between the temporal duration of the dipolarization and the observed distance from Earth no clear pattern is found.

In Figure 3.5A the histogram of the boundary size normalized by the proton gyro radius is shown and in Figure 3.5B the histogram of the boundary size normalized by the ion inertial length. From the 24 dipolarization events 15 events have an angle $\alpha < 90°$ (marked blue), and 9 events have an angle $\alpha > 90°$ (marked red). Since the total number of events of these two groups is quite different, the vertical axis in both plots has been normalized with the total number of events. For most of the events the estimated thickness of the front is between 1-3 proton gyro radius and independent of $\alpha$. On the other hand the front thickness for most of the events with $\alpha < 90°$ is less than 3 ion inertial lengths and for the events with $\alpha > 90°$ no significant information

can be obtained.

In Figure 3.6 the estimated thicknesses of the dipolarization fronts are scaled to the plasma inertial length. For the 15 events with an angle $\alpha < 90°$, the ratio $\delta_D/l_{int}$ is not exceeding a factor of 4. The median of the ratio of these 15 events is $\sim 1.5$. For the 9 events with an angle $\alpha > 90°$ three events have a much higher $\delta_D/l_{int}$ ratio but do not exceed a factor of 5. The median of the ratio for these 9 events is $\sim 1.9$. The dashed vertical line is the boundary between the two velocity bins. The horizontal red line is the median of the ratio $\delta_D/l_{int}$ of all 24 dipolarization events and is $\sim 1.8$. The horizontal green lines are the upper and lower quartiles ($\sim 2.5$ and $\sim 1.0$). The circles mark the two events from Figure 3.2. The event from 29 August 2003 has a magnetic boundary size of $\sim 970 \pm 240$ km, a inertial length of $\sim 370 \pm 60$ km and hence a factor of $\sim 2.5$. The event from 1 October 2003 has a magnetic boundary size of $\sim 1060 \pm 270$ km, an inertial length of $\sim 260 \pm 60$ km and hence a factor of $\sim 4$ (see Figure 3.6).

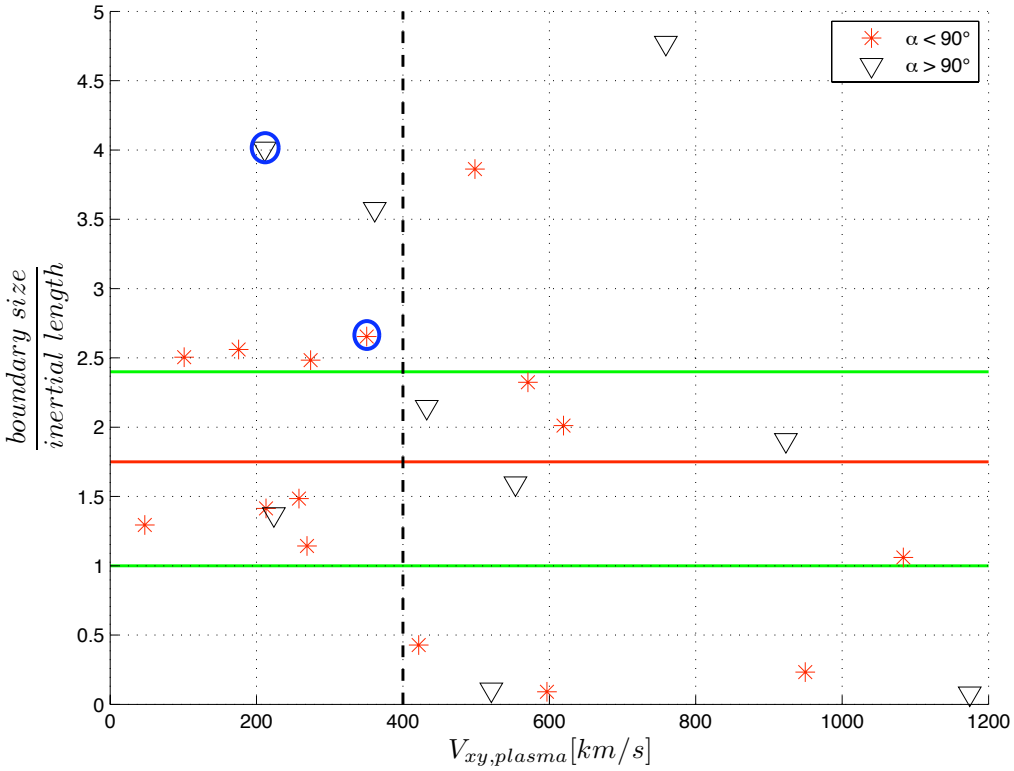


Figure 3.6: Ratio of the estimated boundary size of the magnetic structure and the inertial length of the protons in the magnetic structure for the evaluated 24 events. $\alpha$ is the angle between the estimated normal velocity of the magnetic structure and the maximum perpendicular plasma flow in $XY$ plane. The 15 dipolarization events with an angle $\alpha < 90°$ are marked by stars. The 9 dipolarization events with an angle $\alpha > 90°$ are marked by triangles. The vertical doted line indicate the 2 velocity bins. The horizontal line is the median of the ratio boundary size and inertial length of the 24 dipolarization events and is about $\sim 1.8$. The horizontal green lines are the upper and lower quartiles of the median. The event from August 8, 2003 is the star, marked by a circle. The event from October 1, 2003 is the triangle, marked by a circle.

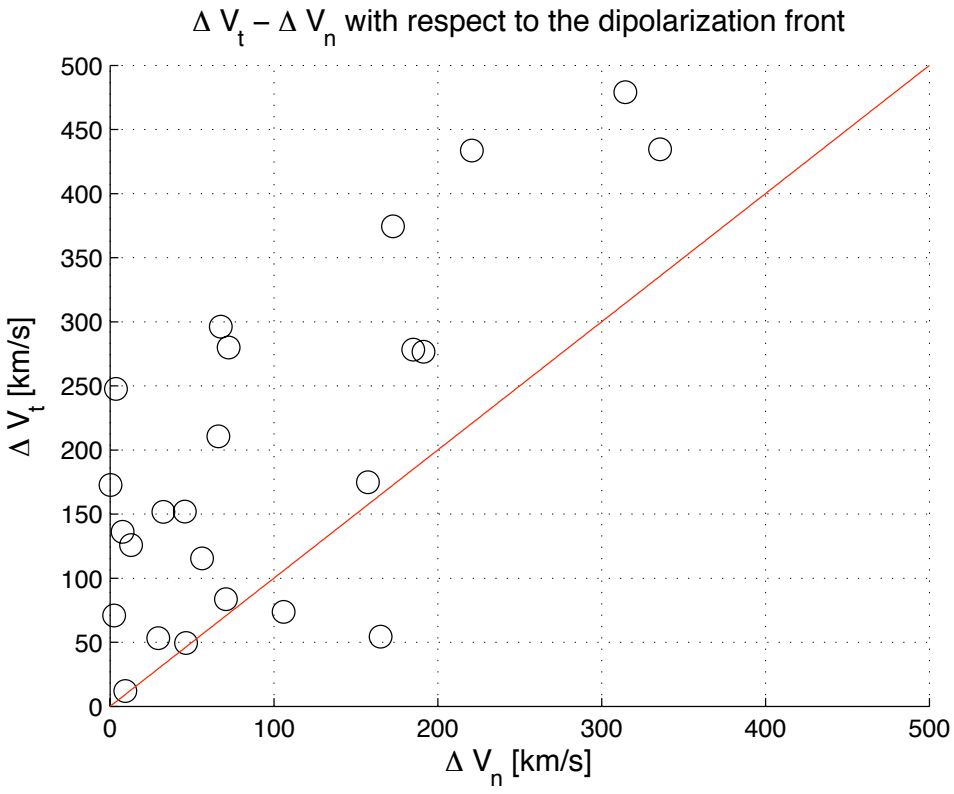


Figure 3.7: Relationship between the perpendicular plasma velocity, the estimated timing velocity and the angle $\alpha$ of the 24 dipolarization events. First we obtained the mean average perpendicular plasma velocity $V_{\perp}$ during the dipolarization (between $B_{z,\mathrm{min}}$ and $B_{z,max}$). Then the velocity difference between the estimated mean plasma velocity and the estimated timing velocity $V_{timing}$ was determined. Then the velocity difference was projected onto the timing velocity vector and the parallel $\Delta V_{\mathrm{t}}$ and perpendicular components $\Delta V_{\mathrm{n}}$ were evaluated and plotted.

Since past studies used the plasma flow velocity in single spacecraft observations to estimate such boundary size [e.g. 25], a scattered plot of the relationship between the perpendicular plasma velocity, the estimated timing velocity and the angle $\alpha$ of the 24 events is given in Figure 3.7. First we obtained the mean average perpendicular plasma velocity $V_{\perp}$ during the dipolarization (between $B_{z,\mathrm{min}}$ and $B_{z,max}$). Then the velocity difference between the estimated mean plasma velocity and the estimated timing velocity $V_{timing}$ was determined. Then the velocity difference was projected onto the timing velocity vector and the parallel $\Delta V_{\mathrm{t}}$ and perpendicular components $\Delta V_{\mathrm{n}}$ were evaluated and plotted. It is often assumed that the dipolarization is a tangential dicontinuity [see e.g., 29], which would mean that $\Delta V$ mainly have tangential component, which is indeed the case for most of the events.

## 3.5 Dipolarization-associated Currents

Any change in magnetic field is associated with current flow and thus it is expected that the dipolarizations found in this master thesis will also show current signatures. We examine the dipolarization-associated currents on different temporal scales. Using the curlometer technique [12] we can deduce the currents from the magnetic fields measured by Cluster.

Figure 3.2 (left panel) shows the magnetic field data (panel D-F) for 29 August 2003, where the separation of the spacecraft was $\sim$ 500 km, and the components of the current are shown too (panel H-J), with the perpendicular part (with respect to the magnetic field at the barycenter of the four spacecraft) shown as a filled region under the curve. On the small scale it can be seen that there is strong perpendicular current in the the $X$ and $Y$ direction after the minimim in $B_z$, and basically in the dipolarization front. This current is responsible for the decrease in $B_z$ preceding the dipolarization front. The estimated thickness of the dipolarization front is $\delta_D \approx 970$ km (or $\sim 2.5$ intertial lengths). This means that we are sampling the current on a scale smaller than the structure itself and at near the inertial length

There is a plasma pressure drop over the dipolarization front from $P_{pl} \approx 0.4$ nPa before to $P_{pl} \approx 0.2$ nPa after the dipolarization front has passed (not shown). This pressure gradient can drive a diamagnetic current through:

$$\mathbf{j}_{dia} = \frac{\mathbf{B} \times \nabla_\perp P_\perp}{B^2}. \tag{3.1}$$

We can estitmate the diamagnetic current assuming: $\nabla_\perp p_\perp \approx \Delta P_{pl}/\delta_D$ along the front normal [see e.g., 26, 37]; the normal of the front is determined by timing analysis $\mathbf{n} \approx (0.13, -0.71, 0.68)$; the magnetic field at dipolarization maximum $\mathbf{B} \approx (-2, 5, 14)$ nT. Using Equation 3.1 we find for the diamagnetic current $\mathbf{j}_{dia} \approx (11, 3, 1)$ nA/m$^2$. This is in the right direction, as can be seen in Figure 3.2A, however, the result is off by a factor of $\sim 2$.

Similarly, we investigate the dipolarization for 1 October 2003, shown in Figure 3.2B. This event shows a much slower dipolarization over $\sim$ 12 sec, with a plasma velocity mainly from the $Z$ direction to the $Y$ direction and a timing velocity $\mathbf{V}_{timing} \approx (-48, -65, 55)$ km/s, i.e. in the tailward direction, corresponding to a physical size of $\sim$ 1070 km. The magnetic field at the $B_z$ peak is $\mathbf{B} \approx (-2, 2, 4)$ nT. The associated diamagnetic current in this case would be $\mathbf{j}_{dia} = (44, -10, 28)$ nA/m$^2$ much higher than measured. However, this is a different kind of diplarization as in the previous event as $\alpha > 90°$. We will investigate this further in the discussion section.

For each of the 24 events we have used the curlometer technique to estimate the current. We have then determined the current parallel and perpendicular to the magnetic field and have produced a scatter plot $j_{||}$ and $j_\perp$, taken at the dipolarization front. In

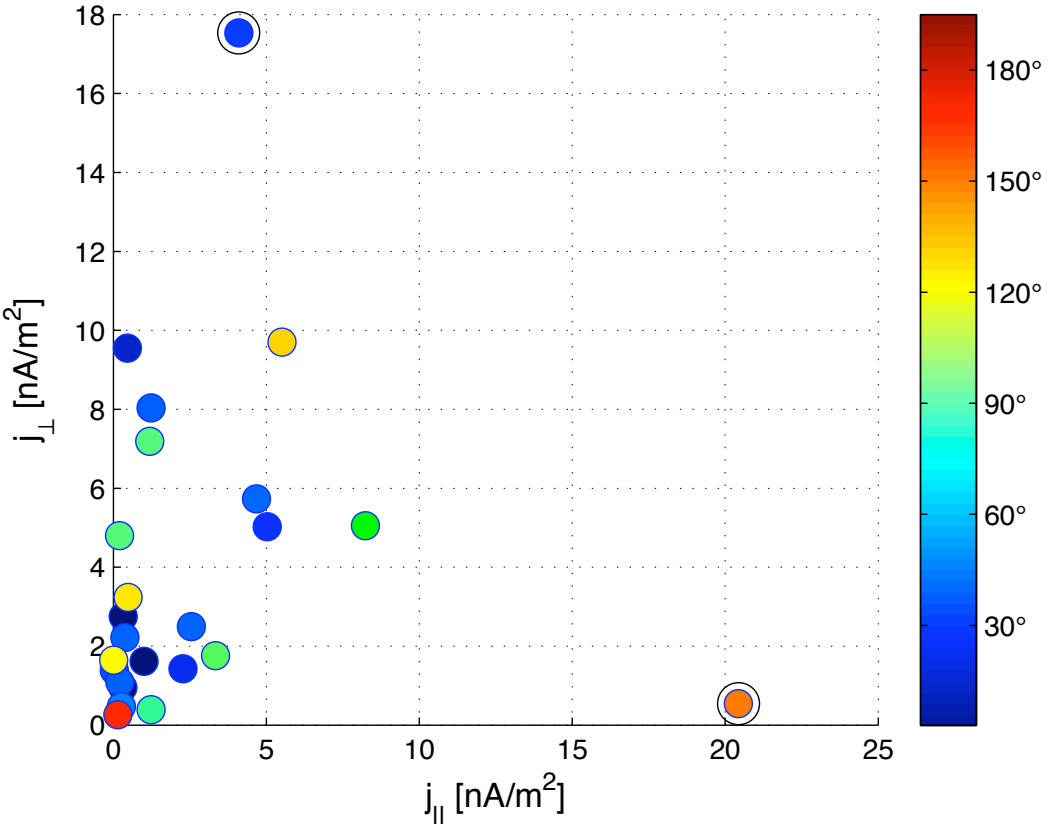


Figure 3.8: Scatter plot between the estimated $j_\perp$ and $j_{||}$, each calculated at $B_{z,min}$, with a color scale showing the angle $\alpha$ of the 24 dipolarization events. The event from 29 August 2003 is the blue dot ($\alpha \approx 30°$) marked by a black circle and the event from 1 October 2003 is the orange dot ($\alpha \approx 150°$) marked by a black circle.

Figure 3.8 the scatter plot between the estimated $j_\perp$ and $j_{||}$, each calculated at the front, with a color scale showing the angle $\alpha$ is shown. The event from 29 August 2003 is the blue dot ($\alpha \approx 30°$) marked by a black circle and the event from 1 October 2003 is the orange dot ($\alpha \approx 150°$) marked by a black circle. This shows that the main current on the dipolarization front is perpendicular to the magnetic field and there seems to be no correlation with $\alpha$. Interestingly the 1 October 2003 event shows a strong deviation from the main characteristic of the rest of the currents.

In a recent paper, Runov et al. [27] discussed the results of a superposed epoch analysis of dipolarization fronts observed from THEMIS. It was found that the current densites associated with the $B_z$ increase are on average 5-7 times larger than the current density in the crosstail. This is in good agreement with our results since the estimated $j_\perp$ for half of the events is greater than 4 nA/m$^2$ and therefore greater than the nominal crosstail current.

# Chapter 4

# Summary and Discussion

In chapter 3 we studied dipolarization fronts observed by the Cluster satellite at $-20$ $R_E \leq X_{GSM} \leq -10$ $R_E$ and $|Y_{GSM}| \leq 12$ $R_E$. Our event selection is based on the perpendicular Earthward plasma flow velocity in $X$ direction $V_{\perp x}$, the elevation angle $\theta$, and it also requires that the spacecraft is in the plasma sheet close to the neutral sheet.

Superposed epoch analysis was performed to examine the duration of the dipolarization front based on 107 dipolarization events. Utilizing high resolution data from all four Cluster spacecraft, we also evaluated the thickness of the dipolarization based on the four spacecraft timing velocity for 24 diplarization events.

From the statistical study, the main results are summarized as follows:

1. The duration of the dipolarization front is found to show a tendency to decrease with increasing velocity of the plasma flow.

2. The thickness of the dipolarization front, is found to be independent of the plasma flow velocity and is on average $\sim 450 \pm 350$ km.

3. The average size of the dipolarization front is in the order of the evaluated ion gyro radius of $\sim 590 \pm 150$ km.

4. The estimated average inertial length of the ions in the magnetic structure is $\sim 340 \pm 60$ km and hence corresponds to the size of the dipolarization front with a factor of $\sim 1.8$.

5. The angle between the Earthward plasma flow direction and dipolarization front motion can either be smaller or greater than 90°, distinguishing between flux transport and flux pile up events.

6. The dipolarization fronts tend to be tangential discontinuities.

7. The currents flowing on the fronts have mainly a perpendicular component to the magnetic field.

The average size for the thickness of the dipolarization front, 450 km, just below the average ion gyro radius and just above the ion inertial length, agrees well with estimates made for case studies by various other authors: Apatenkov et al. [4] showed a thickness of 400-500 km, whereas Runov et al. [25] found that the thickness was on the order of the ion inertial length. However, Nakamura et al. [20] showed a thickness of 2000 km for one event. The variation in thickness of the events in this paper vary between 0.2 and 4 ion inertial lengths, and it may well be that it depends on parameters that have not yet been taken into account, e.g. the current sheet composition and the current sheet thickness.

Two dipolarization events (out of the 24) were looked at in more detail. These events showed that for one, the Earthward moving dipolarization with $\alpha \approx 30°$, the magnetic structure could be well described by the diamagnetic currents flowing on the front. However, for the other event, with tailward moving dipolarization at $\alpha \approx 150°$, the estimated diamagnetic current did not fit the data. Indeed the current during this dipolarization is more parallel than perpendicular to the magnetic field. This seems to be a special case in the 24 events that were looked at, as all other events much smaller parallel currents.

The dipolarizations in this study can be divided into two groups, according to the angle between the plasma flow direction and the magnetic field motion direction, with the angle $\alpha$ either smaller or larger than 90°. There is the expected category, in which the plasma and the magnetic field move in the same direction, and the dipolarization that is observed comes from the relaxation of the magnetic tension in the stretched field lines as they move Earthward. These dipolarizations occur when there is unimpeded flow.

The other category is when the plasma flow is Earthward but the dipolarization motion is tailward. This means that there is a pileup of the magnetic field in the tail. One would expect that the plasma flow would be deflected by the barrier which causes the pileup. Indeed, in the event on 1 October 2003 (see Figure 3.2B) shows that the plasma flow is indeed deflected towards the dawn side of the tail (large $V_y$).

The diamagnetic current that was found for the 29 August event (see Figure 3.2A), was in good agreement with theory, and it flows over an interval of $\sim 4$ s, which corresponds to a physical size of $\sim 1000$ km, just over 2 times the ion inertial length (see Figure 3.6). Zhou et al. [38] found that the thickness of the current layer was just below one ion inertial length, however, their event happened much closer to the Earth at $X \geq -10R_E$, where the conditions may be different because of the more dipolar like magnetic field structure.

Further investigation of these structures is necessary and planned to investigate the dependences of the thickness of the dipolarization on various parameters in the Earth's magnetotail and to study the large scale development of these structures in the tail and their possible role in the braking of the associated flow.

# Appendix A

# Mathematical Basics

## A.1 Useful Constants

As in this master thesis, the values of the constants are given in SI units.

| | | |
|---|---|---|
| $c_0$ | velocity of light in vacuum | $3 \cdot 10^8$ m/s |
| $\mu_0$ | free space magnitic permeability | $4\pi \cdot 10^{-7}$ H/m |
| $\varepsilon_0$ | vacuum dielectric constant | $8.85 \cdot 10^{-12}$ F/m |
| $e$ | electron charge | $1.60 \cdot 10^{-19}$ C |
| $m_e$ | electron mass | $9.11 \cdot 10^{-31}$ kg |
| $m_p$ | proton mass | $1.67 \cdot 10^{-27}$ kg |
| $k_B$ | Botzmann's constant | $1.38 \cdot 10^{-23}$ J/K |
| $R_0$ | ideal gas constant | 8.31 J $K^{-1}$ $mol^{-1}$ |
| $R_E$ | equatorial radius of Earth | $6.37 \cdot 10^6$ m |

Table A.1: Useful constants [1].

[1] Source: [6]

## A.2 Energy Units

Because thermal energy and temperture are related by $W = k_B T$, Joule and Kelvin are often used interchangeably. However, particle energy is often measured in eV. the three units are related as follows:

| | | | |
|---|---|---|---|
| 1 J | - | $7.24 \cdot 10^{22}$ K | $6.24 \cdot 10^{18}$ eV |
| 1 K | $1.38 \cdot 10^{-23}$ J | - | $8.62 \cdot 10^{-5}$ eV |
| 1 eV | $1.60 \cdot 10^{-19}$ J | $1.16 \cdot 10^{4}$ K | - |

Table A.2: Energy Units

## A.3 Differential Relations

The vector derivatives tensors used in this master thesis obey the following rules:

$$\nabla \times \mathbf{A} \times \mathbf{B} = \mathbf{A}(\nabla \cdot \mathbf{B}) - \mathbf{B}(\nabla \cdot \mathbf{A}) + (\mathbf{B} \cdot \nabla)\mathbf{A} - (\mathbf{A} \cdot \nabla)\mathbf{B} \quad \text{(A.1)}$$

$$\nabla^2 \mathbf{A} = \nabla(\nabla \cdot \mathbf{A}) - \nabla \times (\nabla \times \mathbf{A}) \quad \text{(A.2)}$$

$$\nabla^2 \mathbf{A} = \nabla(\nabla \cdot \mathbf{A}) - \nabla \times (\nabla \times \mathbf{A}) \quad \text{(A.3)}$$

$$\nabla \cdot (\mathbf{AB}) = (\mathbf{A} \cdot \nabla)\mathbf{B} + \mathbf{B}(\nabla \cdot \mathbf{A}) \quad \text{(A.4)}$$

$$\nabla \times (\mathbf{AB}) = (\nabla \times \mathbf{A})\mathbf{B} - (\mathbf{A} \times \nabla)\mathbf{B} \quad \text{(A.5)}$$

$$\nabla \cdot (\nabla \times \mathbf{A}) = 0 \quad \text{(A.6)}$$

## A.4 Maxwell Equations

| | |
|---|---|
| **Gauss's law** | $\nabla \cdot \mathbf{E} = \frac{\rho}{\varepsilon_0}$ |
| **Gauss's law for magnetism** | $\nabla \cdot \mathbf{B} = 0$ |
| **Maxwell-Faraday equation** (Faraday's law of induction) | $\nabla \times \mathbf{E} = -\frac{\partial \mathbf{B}}{\partial t}$ |
| **Ampere's circuital law** (with Maxwell's correction) | $\nabla \times \mathbf{B} = \mu_0 \mathbf{j} + \mu_0 \varepsilon_0 \frac{\partial \mathbf{E}}{\partial t}$ |

Table A.3: Maxwell equations

## A.5 Least Squares Fits

In section 3.4 we use a least squares fit for the timing analysis to determine the velocity $\mathbf{v}$ of the boundary plane, which is moving along its normal direction $\hat{\mathbf{n}}$. The input data are values of the separation distances of the four spacecraft, $\mathbf{x}$. This values are related to the velocity, $\mathbf{v}$, by the matrix $\mathbf{T}$, the time difference from the boundary pass from one SC to another.
With the error defined as $\mathbf{e} = (\mathbf{Tv} - \mathbf{x})$, a least squares fit requires us to minimize the square sum of $E = \mathbf{e}^T\mathbf{e}/2$ (where the superscript $T$ indicates the transpose) with respect to the unknown parameter $\mathbf{v}$ of the model. This requires $dE/d\mathbf{v} = 0$. The velocity $\mathbf{v}$ is then the solution of

$$\begin{aligned} \frac{d}{d\mathbf{x}}\frac{1}{2}(\mathbf{Tv}-\mathbf{x})^T(\mathbf{Tv}-\mathbf{x}) &= \frac{1}{2}\mathbf{T}^T(\mathbf{Tv}-\mathbf{x}) + \frac{1}{2}(\mathbf{Tv}-\mathbf{x})^T\mathbf{T} \\ &= \mathbf{T}^T(\mathbf{Tv}-\mathbf{x}) = 0 \end{aligned}$$

which by matrix inversion gives

$$\boxed{\mathbf{v} = (\mathbf{T}^T\mathbf{T})^{-1}\mathbf{T}^T\mathbf{x}} \tag{A.7}$$

# Appendix B

# Glossary

This Glossary is mainly based on the defining dictionary of Suess and Tsurutani [31].

**Adiabatic Invariant:** In a nearly collisionless, ionized gas, electrically charged particles orbit around magnetic lines of force. Certain physical quantities are approximately constant for slow (adiabatic) changes of the magnetic field n time or in space and there quantities are called *adiabatic invariants*.

**Anisotropic Plasma:** A plasma whose properties vary with direction relative to the ambient magnetic field direction. This can be due to e.g. the presence of a magnetic or electric field.

**Beta** (plasma-beta): The ratio of the thermal pressure to the magnetic 'pressure' in a plasma - $\frac{p}{B^2/8ß}$ in cgs-units.

**Bow Shock** (Earth): A collisionless shock wave i front of the magnetosphere arising from the interaction of the supersonic solar wind with the Earth's magnetic field.

**Convection** (plasma, magnetospheric): The bulk transport of plasma (or gas) from one place to another, in response to mechanical forces (e.g. viscous interaction with the solar wind) or electromagnetic forces. Magnetospheric convection is driven by the dragging of the Earth's magnetic field and plasma together by the solar wind when the geomagnetic field becomes attached to the magnetic field in the solar wind.

**Corotating** (with the Earth): A plasma in the magnetosphere of the Earth is said to be corotating with the Earth if the magnetic field drags the plasma with it and together they have a 24 hour rotation period.

**Cyclotron Frequency:** When a particle of charge $q$ moves in a magnetic field **B**, the particle orbits, or gyrates around the magnetic field lines. The cyclotron frequency is the frequency of this gyration, and is given by $\omega_C = \frac{q|B|}{mc}$, where m is the mass of the particle, and c the velocity of light (in cgs-units).

**Drift** (of ions/electons): As particles gyrate around magnetic field lines, their orbits may "drift" perpendicular to the local direction of the magnetic field. This occurs if there is a force also perpendicular to the field - e.g. an electric field, curvature in the magnetic field direction or gravity.

**Electron Volt:** The kinetic energy gained by an electron or proton being accelerated in a potential drop of 1 Volt.

**Energetic Particle:** Energetic particles are defined relative to the background Thermal Plasma s o that any particle having a larger energy than the thermal energy is an energetic particle.

**Field Aligned Current:** A current flowing along (or opposite to) the magnetic field direction.

**Flux Rope:** A magnetic phenomenon which has a force-free field configuration.

**Frozen-in Field:** In a tenuous, collisionless plasma, the weak magnetic fields embedded in the plasma are convected with the plasma. i.e., the are "frozen-in".

**Gyration** (gyroscopic motion): The circular motion of a charged particle i a magnetic field.

**Gyroradius:** The radius of motion of a charged particle about magnetic field line.

**Interplanetary Magnetic Field - IMF:** The magnetic field carried with the solar wind and twisted into an Archimedean spiral by the Sun's rotation.

**Interplanetary Medium:** The volume of space in the solar system that lies between the Sun and the planets. The solar wind flows in the interplanetary medium.

**Interstellar Medium:** The volume of the galaxy (the milky way) lying between stars.

**Ionosphere:** The region of the Earth's upper atmosphere containing free electrons and ions. this ionization is produced from the neutral atmosphere by solar ultraviolet radiation at very short wavelengths ($< 100$ nm) and also by precipitating energetic particles.

**Magnetic Diffusion:** The slow stochastic motion of the particles .

**Magnetic Drift:** Slow motion of magnetic field regions on the surface of a body of plasma, where a magnetic field line enters the surface.

**Magnetic Reconnection:** The act of interconnection between oppositely directed magnetic field lines.

**Magnetopause:** The boundary surface between the solar wind and the magnetosphere, where the pressure of the magnetic field of the object effectively equals the ram pressure of the solar wind plasma.

**Magnetosheath:** The region between the bow shock and the magnetopause, chracterized by vry turbulent plasma. This plasma has been heated (shocked) and slowed as it passed though the bow shock. For the Earth, along the Sun-Earth axis, the magnetosheath is about 3 Earth radii thick.

**Magnetotail:** The extension of the magnetosphere in the antisunward direction as a result of interaction with the solar wind. In the inner magnetotail, the field lines maintain a roughly dipolar configuration. But at greater distances in the antisunward direction, the field lines are stretched into northern and southern lobes, separated by a plasmasheet. there is observational evidence for traces of the Earth's magnetotail as far as 1000 Earth radii downstream, in the antisolar direction.

**Plasma** (ions, electrons): A gas that is sufficiently ionized so as to affect its dynamical behaviour. A plasma is a good electric conductor and is strongly affected by

magnetic fields.

**Plasma Frequency:** The natural frequency of oscillation of electrons in a neutral plasma (e.g. equal numbers of electrons and protons).

**Plasma Sheet:** A region in the center of the magnetotail between the north and south lobes. The plasma sheet is characterized by hot, dense plasma and is a hight beta plasma region, in contrast to the low beta lobes. the plasma sheet bounds the neutral sheet were the magnetic field direction reverses from Earthward (north lobe direction) to anti-Earthward (south lobe direction).

**Radiation Belt:** Regions of the magnetosphere roughly 1.2 to 6 Earth radii above the equator in which charged particles are stably trapped by closed geomagnetic field lines. There are two belts. The inner belt's maximum proton density lies near 5000 km above the Earth's surface. inner belt protons have high energy (MeV range) and originate from the decay of secondary neutrons created during collisions between cosmic rays and upper atomospheric particles. The outer belt extends on to the magnetopause on the sunward side (10 Earth radii under normal quiet conditions) and to about 6 Earth radii on the nightside. the altitude of maximum proton density is near 16000-20000 km. Outer belt protons are lower energy (about 200 eV to 1 MeV). The origin of the particles (before they are energized to these high energies) is a mixture of the solar wind and the ionosphere. The outer belt is also characterized by highly variable fluxes of energetic electrons. The radiation belts are often called the "Van Allen radiation belts" because they were discovered in 1958 by a research group at the University o Iowa led b Professor J.A. Van Allen.

**Reconnection:** A process by which differently directed field lines link up, allowing topological changes of the magnetic field to occur, determining patterns of plasma flow, and resulting in conversion of magnetic energy to kinetic and thermal energy of the plasma. Reconnection is invoked to explain the energization and acceleration of the plasmas/ energetic particles that are observed in solar flares, magnetic substorms and storms, and elsewhere in the solar system.

**Ring Current:** In the magnetosphere, a region of current that flows near the geomagnetic equator in the outer belt of the two Van Allen radiation belts. The current is produced by the gradient and curvature drift of the trapped charged particles of energies of 10 to 300 keV.

**Solar Wind:** the outward flow of solar particles and magnetic fields from the Sun. Typically solar wind velocities are 300-800 km/s and proton and electron densities of 3-7 per cubic centimeter (roughly inversely correlated with velocity). The total intensity of the IMF is nominally 3-8 nT.

**Substrom:** A substorm, sometimes referred to as a magnetospheric substorm or an auroral substorm, is a brief disturbance in the Earth's magnetosphere that causes energy to be released in the "tail" of the magnetosphere. It corresponds to an injection of charged particles from the magnetotail into the nightside magnetosphere. Plasma instabilities lead to the precipitation of the particles into the auroral zone ionosphere, producing intense aurorae.

# Bibliography


[1] Angelopoulos, V.: The THEMIS mission, Space Sci. Rev., 141, 5 Ű 34, 2002.

[2] Angelopoulos, V., Baumjohann, W., Kennel, C. F., Coroniti, R. V., Kivelson, M. G., Pellat, R., Walker, R. J., Lühr, H., and Paschmann, G.: Bursty bulk flows in the inner central plasma sheet, J. Geophys. Res., 97, 4027–4039, 1992.

[3] Angelopoulos, V., Kennel, C. F., Coroniti, F. V., Pellat, R., Kivelson, M. G., Walker, R. J., Russell, C. T., Baumjohann, W., Feldman, W. C., and Gosling, J. T.: Statistical characteristics of bursty bulk flow events, J. Geophys. Res., 99, 21 257–21 280, 1994.

[4] Apatenkov, S. V., Sergeev, V. A., Kubyshkina, M. V., Nakamura, R., Baumjohann, W., Runov, A., Alexeev, I., Fazakerley, A., Frey, H., Mühlbachler, S., Daly, P. W., Sauvaud, J.-A., Ganushkina, N., Pulkkinen, T., Reeves, G. D., and Khotyaintsev, Y.: Multi-spacecraft observation of plasma dipolarization/injection in the inner magnetosphere, Ann. Geophys., 25, 801Ű814, 2007.

[5] Balogh, A., Carr, C. M., Acuña, M. H., Dunlop, M. W., Beek, T. J., Brown, P., Fornacon, K.-H., Georgescu, E., Glassmeier, K.-H., Harris, J., Musmann, G., Oddy, T., and Schwingenschuh, K.: The Cluster magnetic field investigation: Overview of inflight perfomance and initial results, Ann. Geophys., 19, 1207–1217, 2001.

[6] Baumjohann, W. and Treumannn, R. A.: Basic Space Plasma Physics, Imperial College Press, London, UK, 1996.

[7] Baumjohann, W., Paschmann, G., and Lühr, H.: Characteristics of high-speed flows in the plasma sheet, J. Geophys. Res., 95, 3801–3809, 1990.

[8] Baumjohann, W., Hesse, M., Kokubun, S., Mukai, T., Nagai, T., and Petrukovich, A. A.: Substorm dipolarization and recovery, J. Geophys. Res., 104, 24,995–25,000, 1999.

[9] Baumjohann, W., Schödel, R., and Nakamura, R.: Bursts of fast magnetotail flux transport, Adv. Space Res., 30, 2241–2246, 2002.

[10] Dubyagin, S., Sergeev, V., Apatenkov, S., Angelopoulos, V., Runov, A., Nakamura, R., Baumjohann, W., McFadden, J., and Larson, D.: Can flow bursts

penetrate into the inner magnetosphere ?, Geophys. Res. Lett., 38, L08102, doi: 10.1029/2011GL047016, 2011.

[11] Escoubet, C. P., Russell, C. T., and Schmidt, R.: The Cluster and Phoenix missions, Kluwer Academic Publishers, Dordrecht, the Netherlands, 1997.

[12] Harvey, C. C.: Spatial gradients and volumetric tensor, in: Analysis Methods for Multi-Spacecraft Data, edited by Paschmann, G. and Daly, P., pp. 307–322, ESA, Noordwijk, 1998.

[13] Heyn, M.: Grundlegende Konzepte der Plasmaphysik, Script for the Plasmaphysics lecture: 515.272, Graz, Styria, Austria, 2010.

[14] Kiehas, S. A., Semenow, V. S., Kubyshkina, M., Angelopoulos, V., Nakamura, R., Keika, K., Ivanova, V. V., Biernat, H. K., Baumjohann, W., Mende, S., Magnes, W., Auster, U., Fornacon, K. H., Larson, D., Carlson, C. W., Bonnell, J., and McFadden, J.: First application of a Petschek-type reconnection model with time-varying reconnection rate to THEMIS observations, J. Geophys. Res., 114, A00C20, doi:10.1029/2008JA013528, 2009.

[15] Laakso, H., Taylor, M., and Escoubet, C.: The Cluster Active Archive - Studying the Earth's Space Plasma Enviroment, Springer, Dordrecht Heidelberg London New York, 2010.

[16] Li, S., Angelopoulos, V., Runov, A., X.-Z-Zhou, McFadden, J., Larson, D., Bonnell, J., and Auster, U.: On the force balance around dipolarization fronts within bursty bulk flows, J. Geophys. Res., 116, A00I35, doi:10.1029/2010JA015 884, 2011.

[17] Lui, A. T. Y., Volwerk, M., Dunlop, M. W., Alexeev, I. V., Fazakerley, A. N., Walsh, A. P., Lester, M., Grocott, A., Mouikis, C., Henderson, M. G., Kistler, L. M., Shen, C., Shi, J. K., Zhang, T. L., and Rème, H.: Near-Earth substorm features from multiple satellite observations, J. Geophys. Res., 113, A07S26, doi: 10.129/2007JA012738, 2008.

[18] M. Yamada, R. K. and H.Ji: Magnetic reconnection, Reviws of Modern Physics, 82, 1–62, 2010.

[19] Nakai, H. and Kamide, Y.: Substorm currents associated with magnetotail magnetic dipolarization: Geotail observations, J. Geophys. Res., 105, 18,781 – 18,792, 2000.

[20] Nakamura, R., Baumjohann, W., Klecker, B., Bogdanova, Y., Balogh, A., Re'me, H., Bosqued, J. M., Dandouras, I., Sauvaud, J.-A., Glassmeier, K.-H., Kistler, L., Mouikis, C., Zhang, T. L., Eichelberger, H., , and Runov, A.: Motion of the dipolarization front during a flow burst event observed by Cluster, Geophys. Res. Lett., 29, 1942, doi:10.1029/2002GL015763, 2002.

[21] Nakamura, R., Baumjohann, W., Mouikis, C., Kistler, L. M., Runov, A., Volwerk, M., Asano, Y., Vörös, Z., Zhang, T. L., Klecker, B., Rème, H., and Balogh, A.: Spatial scale of high-speed flows in the plasma sheet observed by Cluster, Geophys. Res. Lett., 31, L09894, doi:10.1029/2004GL019558, 2004.

[22] Ohtani, S., Shay, M. A., and Mukai, T.: Temporal structure of the fast convective flow in the plasma sheet: Comparison between observations and two-fluid simulations, J. Geophys. Res., 109, 3–8, doi:10.1029/2003JA010002, 2004.

[23] Paschmann, G. and Daly, P.: Analysis Methods for Multi-Spacecraft Data, ESA, Noordwijk, 1998.

[24] Rème, H., Aostin, C., Bosqued, J. M., Danduras, I., Lavraud, B., Sauvaud, J.-A., Barthe, A., Bouyssou, J., Camus, T., Coeur-Joly, O., et al.: First multispacecraft ion measurements in and near the Earth's magnetosphere with the identical Cluster ion spectrometry (CIS) experiment, Ann. Geophys, 19, 1303–1354, 2001.

[25] Runov, A., Angelopoulos, V., Sitnov, M. I., Sergeev, V. A., Bonnell, J., McFadden, J. P., Larson, D., Glassmeier, K.-H., and Auster, U.: THEMIS observations of an earthward-propagating dipolarization front, Geophys. Res. Lett., 36, L14106, doi:10.1029/2009GL038980, 2009.

[26] Runov, A., Angelopoulos, V., Sitnov, M., Sergeev, V., Nakamura, R., Nishimura, Y., Frey, H., McFadden, J., Larson, D., Bonnell, J., Glassmeier, K.-H., Auster, U., Connors, M., Russell, C., and Singer, H.: Dipolarization fronts in the magnetotail plasma sheet, Planet. Space Sci., doi:10.1016/j.pss.2010.06.006, 2010.

[27] Runov, A., Angelopoulos, V., Zhou, X.-Z., Zhang, X.-J., Li, S., Plaschke, F., and Bonnell, J.: A THEMIS multicase study of dipolarization fronts in the magnetotail plasma sheet, J. Geophys. Res., 116, A05 216, doi:10.1029/2010JA016 316, 2011.

[28] Sergeev, V., Angelopulous, V., Carlson, C., and Sutcliffe, P.: Current sheet measurements within a flapping plasma sheet, J. Geophys. Res., 103, 9177–9188, 1998.

[29] Sergeev, V. A., Angelopoulos, V., Gosling, J. T., Cattell, C. A., and Russell, C. T.: Detection of localized, plasma-depleted flux tubes or bubbles in the midtail plasma sheet, J. Geophys. Res., 101, 10,817 – 10,826, 1996.

[30] Sigsbee, K., Slavin, J. A., Lepping, R. P., A.Szabo, Øierset, M., Kaiser, M. L., Reiner, M. J., and Singer, H. J.: Statistical and superposed epoch study of dipolarization events using data from Wind perigee passes, Ann. Geophys., 23, 832–834, 2005.

[31] Suess, S. T. and Tsurutani, B. T.: From the Sun: Auroras, Magnetic Storms, Solar Flares, Cosmic Rays, American Geophysical Union Books Board, Washington, DC, USA, 1998.

[32] Takada, T., Nakamura, R., Baumjohann, W., Asano, Y., Volwerk, M., Zhang, T. L., Klecker, B., Rème, H., Lucek, E. A., and Carr, C.: Do BBFs contribute to inner magnetosphere dipolarizations: Concurrent Cluster and Double Star observations, Geophys. Res. Lett., 33, L21109, doi:10.1029/2006GL027440, 2006.

[33] Volwerk, M.: Multi-Satellite observations of ULF waves, in: Magnetospheric ULF waves: Synthesis and new directions, edited by Takahashi, K., Chi, P. J., Denton, R. E., and Lysak, R. L., pp. 109 – 135, AGU, Washingtong, 2006.

[34] Volwerk, M., Nakamura, R., Baumjohann, W., Treumann, R. A., Runov, A., Vörös, Z., Zhang, T. L., Asano, Y., Klecker, B., Richter, I., Balogh, A., and Rème, H.: A statistical study of compressional waves in the tail current sheet, J. Geophys. Res., 108, 1429, doi:10.1029/2003JA010155, 2003.

[35] Volwerk, M., Baumjohann, W., Glassmeier, K.-H., Nakamura, R., Zhang, T. L., Runov, A., Vörös, Z., Klecker, B., Treumann, R. A., Bogdanova, Y., Eichelberger, H.-U., Balogh, A., and Rème, H.: Compressional waves in the EarthŠs neutral sheet, Ann. Geophys., 22, 303–315, 2004.

[36] Volwerk, M., Lui, A. T. Y., Lester, M., Walsh, A. P., Alexeev, I., Cao, X., Dunlop, M. W., Fazakerley, A. N., Grocott, A., Kistler, L., Lun, X., Mouikis, C., Pu, Z., Shen, C., Shi, J. K., Taylor, M. G. G. T., Baumjohann, W., Nakamura, R., Runov, A., Vörös, Z., Zhang, T. L., Takada, T., Rème, H., Klecker, B., and Carr, C. M.: Magnetotail dipolarization and associated current systems observed by Cluster and Double Star, J. Geophys. Res., 113, A08S90, doi:10.1029/2007JA012729, 2008.

[37] Zahng, X.-J. and V. Angelopoulos, A. Runov, X.-Z. Z. J. B. J. M. D. L. U. A.: Current-carriers near dipolarization fronts in the magnetotail: A THEMIS event study, J. Geophys. Res., 2010.

[38] Zhou, M., Ashour-Abdalla, M., Deng, X., Schriver, D., El-Alaoui, M., and Pang, Y.: THEMIS observation of multiple dipolarization fronts and associated wave characteristics in the near-Earth magnetotail, Geophys. Res. Lett., 36, L20107, doi:10.1029/200gGL040663, 2009.